

Scientific paper

In Silico Exploration of Molecular Mechanisms for Inhibiting Inflammatory Responses by 3H-Thiazolo[4,5-*b*]pyridin-2-one Derivatives

Olena Klenina^{1,2,*} 

¹ Danylo Halytsky Lviv National Medical University, Faculty of Pharmacy, Department of General, Bioinorganic, Physical and Colloidal Chemistry, 69 Pekarska Str. Lviv, 79010, Ukraine

² San Pablo CEU University, Faculty of Pharmacy, Department of Chemistry and Biochemistry, Urbanización Montepríncipe, 28668 Boadilla del Monte, Spain

* Corresponding author: E-mail: olena.klenina@ceu.es; olena_klenina@yahoo.com
Phone: +380 98-051-9298; +34 674170236

Received: 03-01-2024

Abstract

Combined *in silico* strategy for molecular mechanisms exploration of a series 3H-thiazolo[4,5-*b*]pyridin-2-ones exhibiting strong anti-exudative action through QSAR analysis, molecular docking and pharmacophore modelling is reported. GA-ML technique was used for QSAR models generation with 2D autocorrelation descriptors. One- and two-parameter regressions revealed that certain structural patterns or heteroatoms contribute mutually to the anti-exudative activity potentiation. Possible action mechanisms were discovered through flexible docking simulations with cyclooxygenase pathway enzymes (COX-1, COX-2, mPGES-1). Docking results indicated the possibility of stable complexes formation with the effective docking scores and proper orientation of ligands within the enzymes active sites. Pharmacophore modelling was carried out using protein-ligand interaction fingerprints methodology. Two- and three-centre 3D pharmacophore queries were constructed. Their analysis indicated the functionality of bicyclic thiazolopyridine scaffold proved by the steric placement of heteroatoms in the corresponding pharmacophore centres.

Keywords: Thiazolo[4,5-*b*]pyridines, COX inhibitors, mPGES-1 inhibitors, QSAR analysis, docking, pharmacophore modelling

1. Introduction

The development of anti-inflammatory drugs occupies an important role in the field of modern pharmacology. Among the different signalling molecules involved in inflammatory stage arachidonic acid (AA) and its metabolites contribute strongly to the development of inflammatory and related symptoms.¹ Arachidonic acid, formed during the release of phospholipids from cell membranes, can be metabolised by the cyclooxygenase or lipoxygenase pathways. The cyclooxygenase pathway of AA metabolism leads to prostaglandin H₂ (PGH₂) formation *via* two successive steps both catalysed by COXs. PGH₂ serves as a precursor for different PG biosynthesis including PGD₂, PGE₂, PGI₂, and TXA₂ depending on the expression of specific terminal synthases. Cyclooxygenases (COX-1 and COX-2) are the key enzymes involved in the arachidonic acid cascade.² Classical non-steroidal anti-inflammatory

drugs (NSAIDs) are diverse group of compounds used for the treatment of inflammation.³ The first generation of NSAIDs exert anti-inflammatory, analgesic, and antipyretic effects through the non-selective inhibition of both COX isoforms. Their use is associated with side effects such as gastrointestinal and renal toxicity.⁴ Selective COX-2 inhibitors (rofecoxib, celecoxib, valdecoxib etc.) were developed as the second generation of NSAIDs with improved gastric safety profile and therefore more safe. Microsomal prostaglandin E synthase-1 (mPGES-1) is the terminal enzyme in PG biosynthesis pathway and catalyses the conversion of PGH₂ to PGE₂.⁵ PGE₂ is a well-characterized mediator of inflammation and pain. Therefore mPGES-1 is a novel attractive target with a low risk of side effects. Very few inhibitors of mPGES-1 were identified in experimental screening efforts. Some novel synthetic mPGES-1 inhibitors among different classes of compounds

were identified in the recent decades by using high-throughput screening (HTS) strategy.⁶ Thus, it is highly desirable to design and discover novel mPGES-1 inhibitors with different scaffolds in order to develop next-generation therapeutics for anti-inflammatory diseases treatment.

Thiazole-based derivatives are actually a considerable group of heterocyclic compounds possessing a significantly broad spectrum of pharmacological actions and therapeutic effects against many pathological states. In the last years the scaffold consisting of thiazole ring linked to pyridine one and functionalized with different fragments has attracted considerable interest due to diverse activities.⁷ A great number of publications have been currently reported thiazolopyridines biological evaluations as potent antihypertensive,⁸ antioxidant,⁹ antifungal,¹⁰ antimicrobial,¹¹ antidiabetic,¹² anti-inflammatory,¹³ tuberculostatic,¹⁴ herbicidal¹⁵ and anticancer agents.¹⁶ Furthermore, fused thiazolopyridine analogues are also known as H₃ receptor antagonists,¹⁷ phosphoinositide 3-kinase inhibitors¹⁸ and glucokinase activators.¹⁹

In the past decade fused thiazole-based derivatives became an integral part of new anti-inflammatory agents' discovery. A wide range of synthetic thiazole-bearing derivatives have been studied for their anti-inflammatory properties including COX-1/COX-2 inhibitory action.²⁰ Mohareb *et al.*²¹ reported the synthesis of eleven series of novel fused thiazoles derived from 2-(2-oxo-2*H*-chromen-3-yl)thiazol-4(5*H*)-one and their anti-inflammatory activity evaluation using a carrageenan-induced paw oedema model. All synthesized compounds showed anti-inflammatory activity in the range of 33–96%. Development of novel benzothiazole moiety compounds as promising COX-1/COX-2 inhibitors was reported by El-Kerdawy *et al.*²² They synthesized a series of new 3-methylbenzo[4,5]imidazo[2,1-*b*]thiazol-2-yl)nicotinoyl)-*N*-substituted derivatives with the aim to evaluate their anti-inflammatory activity and mechanism of action. The anti-inflammatory activity of this compounds performed by carrageenan-induced mouse paw oedema was in range of 49.0–79.5%. Also, evaluation of COX-1/COX-2 inhibition was performed which revealed non-selective inhibitory activity of benzimidazothiazoles towards both COX isoforms with some compounds being more potent compared to celecoxib and naproxen. Some novel benzyloxybenzo[*d*]thiazole and phenoxyethoxybenzo[*d*]thiazole analogues were synthesized and evaluated *in vivo* as potential anti-inflammatory and analgesic agents.²³ These derivatives were recognized as promising starting points for the development of COX-2 selective inhibitors.

Thiazole scaffold may be also looked through as an attractive pharmacological profile for the further rational design and discovery of novel mPGES-1 inhibitors as safe and potent NSAIDs. Ongoing efforts are made to identify alternate action modes of thiazole-scaffold bearing compounds which may feasibly lead to reduced PGE₂ level. Smith *et al.*²⁴ reported the inhibitory activity of 2-amino-

thiazole derivatives directed to PGE₂ production decreasing. A series of 2-aminothiazole congeners was synthesized and tested for the ability to reduce the production of PGE₂ in HCA-7 cells. A total of 36 aminothiazoles were evaluated, and active compounds with limited COX-2 inhibition were identified. One of the derivatives exhibited the most potent cellular PGE₂ reducing activity of the entire series (EC₅₀ = 90 nM) with IC₅₀ value for COX-2 inhibition of >5 μM *in vitro*. Identification of novel dual LOX/mPGES-1 inhibitors as 2-aminothiazole-featured pirinixic acid derivatives was also reported,²⁵ one compound among them suppressed mPGES-1 (IC₅₀ = 0.4 μM) and 5-LOX (IC₅₀ = 0.3 μM) in cell-free assays.

In the present study we propose a combined *in silico* approach, based on efficient multistep virtual screening workflow, which may accelerate and facilitate the identification of novel selective COX-2 and mPGES-1 inhibitors among fused thiazole-scaffold bearing compounds.

2. Materials and Methods

2.1. QSAR Study

2D structures of all molecules were drawn with ACD/ChemSketch chemical drawing software package. Later on, they were converted to 3D structures using Hyper-Chem 7.5 software.²⁶ Energy minimization of all compounds was performed with MM+ force field, and repeated minimization was performed using semi-empirical AM1 quantum-chemical method until the root-mean-square (rms) deviation of 0.01 kcal/mol would be achieved. Conformations of compounds were optimized through semi-empirical AM1 method with the global minimum selection among all energy-minimal conformers. 3D globally minimized structures as hin HyperChem output were converted into smi format, SD file was prepared with E-BABEL on-line version and utilized as the input for E-DRAGON software.²⁷ Molecular descriptors were calculated within 20 subsets, constant and near constant values of descriptors were discarded, and finally over 1666 descriptors were saved and further analyzed. Descriptors with pairwise correlation coefficient exceeding 0.5, determined based on the correlation matrix analysis, were excluded from the descriptor general set. Before starting the construction of the models, the descriptor normalization procedure was carried out, the values of all generated descriptors were scaled as (1):

$$X_{ij}^n = \frac{X_{ij} - X_{j,\min}}{X_{j,\max} - X_{j,\min}} \quad (1)$$

where X_{ij} and X_{ij}^n are the original and normalized values of the descriptor j ($j = 1, 2, \dots, K$) for i^{th} compound ($i = 1, 2, \dots, 32$), respectively; $X_{j,\min}$ and $X_{j,\max}$ are the minimal and the maximal values for the j^{th} descriptor. Thus, for all normalized descriptors the following criteria are true: $\min(X_{ij}^n) = 0$ and $\max(X_{ij}^n) = 1$. As a result, a set of 482 normalized descriptors for all compounds was prepared.

In order to obtain a validated and predictive QSAR models, we splitted the parent data set into the training and test (validation) ones with the activity ranking algorithm²⁸ in the ratio 27:9, that is the training set consisted of 27 compounds (75% of all) while the validation set contained 9 compounds (25%).

The training set was used in developing QSAR models with BuildQSAR software application²⁹ where the biological activity as % protection to inflammation converted to logarithmic value (log %) served as the dependent variable, and the normalized molecular descriptors were independent variables. In this work, the selection of the optimal set of molecular descriptors was carried out using genetic algorithm (GA) for searching the best models and was processed in the terms of the highest correlation coefficient and *F*-test as well as the lowest standard deviation. Variables selection was carried out within each of descriptors' modules namely 0D-, 1D-, 2D, 3D and module "Other" using previously reported approach.³⁰ Multiple Linear Regression (MLR) method was applied to perform the statistical processing of the QSAR structure-anti-exudative activity models generation.

The statistical significance of the generated models was determined by examining the coefficient of determination R^2 , standard deviation s , the value of the Fisher test F . Adjusted regression coefficient R^2_{adj} was used to ensure that all independent variables (predictors) contribute with the equal significance to explain dependent (target) variable. R^2_{adj} was defined as (2):³¹

$$R^2_{adj} = 1 - \frac{(1-R^2)(n-1)}{n-p-1} \quad (2)$$

where n is the total set size (the total number of observations), p is the number of independent variables (the number of descriptors in the model), and $n-p-1$ is the residual degree of freedom.

Sum of squares for the regression ($SS_{regression}$ or SSR) was estimated as the sum of the differences between the predicted value of the activity $Y_{i\ pred}$ and the mean of the dependent variable for the training set compounds $\bar{Y}_{training}$ (3), while the Mean square for the regression ($MS_{regression}$ or MSR) was an estimate of the variance of the regression (4):

$$SSR = \sum_{i=1}^n (Y_{i\ pred} - \bar{Y}_{training})^2 \quad (3)$$

$$MSR = SSR / DF_{regression} \quad (4)$$

where $DF_{regression}$ is the degree of freedom for the regression: $DF_{regression} = p$.

As the cross-validation coefficients are used as criteria of both robustness and predictive ability of the generated QSAR models, we performed both internal and external cross-validation procedure in the present study. The internal validation of the models was examined using the leave-one-out (LOO) cross-validation method with the

training set compounds. In the LOO cross-validation procedure, every compound was eliminated from the training dataset once and its activity was then predicted as a weighted average of the activities of its nearest neighbours using formula 5:^{32,33}

$$Q^2_{LOO} = 1 - \frac{\sum (Y_{i\ exp} - Y_{i\ calc})^2}{\sum (Y_{i\ exp} - \bar{Y}_{exp})^2} \quad (5)$$

where $Y_{i\ exp}$ and $Y_{i\ calc}$ are the experimental and calculated values of biological activity for molecule i of the training set, respectively; \bar{Y}_{exp} is the mean value of the dependent variable (log %). The summation in this and all the following equations are done over all n compounds of the training set.

For the external validation, the group-one-out cross-validation coefficient Q^2_{LGO} with the test set compounds was calculated using formula 6:³⁴

$$Q^2_{LGO} = 1 - \frac{\sum (Y_{i\ exp(test)} - Y_{i\ calc(test)})^2}{\sum (Y_{i\ exp(test)} - \bar{Y}_{training})^2} \quad (6)$$

where $Y_{i\ exp(test)}$ and $Y_{i\ calc(test)}$ are the activity values for the validation set compounds, observed and predicted with the corresponding model, respectively; and $\bar{Y}_{training}$ is the mean value of the experimental activity of the training set compounds only.

2. 2. Molecular docking studies

All the computational studies were carried out using Molecular Operating Environment Suite 2012.10 (MOE); Chemical Computing Group Inc. software.^{35,36}

Construction and preparation of ligands database

The minimized 3D geometries of all compounds obtained using the HyperChem 7.5 software for QSAR analysis were then converted into SD File format with Open Babel version 2.3.2³⁷ and were used as the input into MOE with a database import function. We firstly generated multiple conformations of each ligand in the database on the systematic search basis. We applied the grid search by rotating each rotatable bond by a fixed angle increment (15° for cyclic, 60° or 120° for acyclic bonds) followed by the conformations' energy minimization with MMFF94x force field and duplicate geometries rejection. The maximum allowed conformations per compound was set to 200 and the energy window (the value used to discard high-energy conformations) was set to 7 kcal/mol. The RMS gradient level was defined as 0.01 kcal/mol/Å², RMSD limit was fixed at 0.25 kcal/mol/Å² while 200 MM iterations were allowed. A data set of 2545 conformations was prepared in the way of systematic search.

Proteins processing and preparation

The X-ray crystallographic structures of the receptors were retrieved from Protein Data Bank (www.rcsb.

org/pdb): 2.0 Å resolution structure of ovine prostaglandin H₂ synthase-1 (COX-1) in complex with α -methyl-4-biphenylacetic acid (PDB code 1Q4G),³⁸ 1.73 Å resolution structure of naproxen-COX-2 complex (PDB entry 3NT1),³⁹ and 1.2 Å resolution structure of human mPGES-1 in complex with glutathione (GSH) (pdb code 4AL0).⁴⁰ They were then loaded into MOE working environment.

The enzymes were prepared for docking studies in a few steps. The receptors' structures were prepared in the way of the partial charges calculation, hydrogens were assigned with the "Protonate3D" function at pH 7.4. Thereafter, residues within a radius of 3 Å around the ions were minimized (AMBER99 force field; RMS gradient 0.01 kcal/mol/Å²). Thus the "Protonate3D" application automatically optimized the hydrogen orientations so as to maximize H-bond networks and minimize the overall self-energy. The binding sites of the proteins were defined by using the "Site Finder" tool in MOE. The co-crystallized ligands were removed from protein-ligand complexes and corresponding ligands locations were set as docking site locations. Site Finder tool was applied for the defined pockets, and „dummy atoms" were created.

Docking studying and scoring

The standard MOE Docking protocol was utilized for the docking studies of the ligands database with COX-1 and COX-2. Residues within a radius of 4.5 Å of the generated "dummy atoms" were selected, Alpha Triangle Poses were generated by superposition of ligand atom triplets and triplets of receptor site points. At each iteration a random conformation was selected, a random triplet of ligand atoms and a random triplet of alpha sphere centres were used to determine the pose. The following docking calculations were performed by means of the DOCK tool implemented in MOE, all obtained docking poses were refined using MMFF94x force field as the default for small molecules in MOE. To reduce the number of poses obtained in this way (865 for COX-1 and 880 for COX-2), the pharmacophore queries were generated. For COX-1 the pharmacophore query with projected H-acceptor feature defined on NH₂ group of Arg 120 residue was generated while two pharmacophore queries with projected H-acceptor features defined on NH₂ and NE groups of Arg 120 side chain residue were consequently generated for COX-2. The docking run procedure was repeated with the first rescoring function setting as "London dG", the refinement scoring function fixing to "GBVI/WSA dG". 357 COX-1-ligand complexes and 412 COX-2-ligand complexes were obtained in this way. The molecular docking studies of the ligands database with mPGES-1 were utilized by setting "GBVI/WSA dG" function for the first rescoring, followed by the addition of a refinement of the resulting complexes with MMFF94x force field and London dG for a second rescoring. 786 mPGES-1-ligand complexes were obtained in this way.

Thereafter, the minimized complexes were scored by the four scoring functions available in MOE: **Affinity dG Scoring** estimated the enthalpic contribution to the free energy of binding, **Alpha HB Scoring** evaluated the geometric fit of the ligand to the binding site and hydrogen bonding effects, **London dG Scoring** and **GBVI/WSA dG Scoring** (forcefield-based) estimated the free energy of binding of the ligand from a given pose. The unit for all scoring functions was kcal/mol. For all scoring functions, lower scores indicated more favourable poses. The docking poses were then expected manually with an eye towards the most proper binding modes verification.

2. 3. Pharmacophore Queries Generation

Protein-ligand interactions fingerprints (PLIF) tool and 3D pharmacophore models generation tool implemented in MOE software were used as a post-processing procedure of docking studies for thiazolo[4,5-*b*]pyridin-2-one derivatives as probable COX-1,2 and mPGES-1 inhibitors. Automatized pharmacophore query generation based on the structural data of protein-ligand complexes obtained from docking studies was a two-step procedure. Firstly, the identification of a protein residues interacting with the ligand was fulfilled, and their summarizing was resulted in the barcode diagram construction in which different types of interactions were given as fingerprints bits. Afterwards MOE's pharmacophore modelling tool determined the most common pharmacophoric feature characteristics that were essential for the binding of ligands to the receptor and their spatial arrangement in 3D. On the final step we validated the fingerprint pharmacophore modelling approach by screening the test database as alignments of molecules on high-scoring pharmacophore queries.

3. Results and Discussion

Recently we reported novel N³ substituted 5,7-dimethyl-6-phenylazo-3*H*-thiazolo[4,5-*b*]pyridin-2-ones synthesis⁴¹ as the integral part of scaffold-based drug-like small molecules design and discovery using traditional organic synthesis protocols and pharmacological screening methodologies.⁴² *In vivo* evaluation of novel thiazolo[4,5-*b*]pyridines over the carrageenin induced rat paw oedema revealed strong anti-exudative activity of some compounds which were comparable or exceeded the effects of Diclofenac and Ibuprofen in their effective therapeutic doses which were tested in parallel as an activity references.

As the focus of our systematic research is aimed at developing the molecular pattern based on 3*H*-thiazolo[4,5-*b*]pyridine scaffold for novel drug candidates construction, the objective of the present study was to perform ligand-based and structure-based virtual screening for recently synthesized 3*H*-thiazolo[4,5-*b*]pyridin-2-ones in

order to apprehend the importance of certain structural features, which are critical for their biological activity accentuation. Thus, a three-step virtual screening protocol was proposed in this work, which included QSAR analysis, molecular docking and protein-ligand complex-based pharmacophore search post-processing.

The set of compounds used in the present study comprises a series of 36 N^3 substituted 5,7-dimethyl-6-phenylazo-3*H*-thiazolo[4,5-*b*]pyridin-2-one derivatives evaluated as anti-exudative agents. Their structures are depicted in Figure 1, while the substituent *R* structures are listed in Table 1. The biological activity data as % protection to inflammation were converted to logarithmic value and subsequently used as the response variable for QSAR analysis.

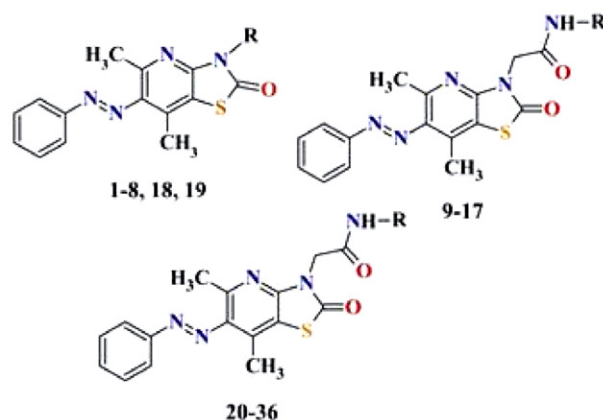


Fig. 1. General structures of N^3 substituted 5,7-dimethyl-3*H*-thiazolo[4,5-*b*]pyridine-2-ones

Table 1. Structures of substituents and anti-exudative effect of 5,7-dimethyl-6-phenylazo-3*H*-thiazolo[4,5-*b*]pyridin-2-ones *in vivo* evaluation, given as % and log % protection from inflammation

Compound ID	<i>R</i>	% Inhibition	log %	Compound ID	<i>R</i>	% Inhibition	log %
1	H	57.2	1.76	20		42.0	1.62
2		54.2	1.73	21		39.2	1.59
3		42.1	1.62	22		36.1	1.56
4		45.1	1.65	23		38.4	1.58
5		47.2	1.67	24		42.0	1.62
6		50.2	1.70	25		45.1	1.65
7		48.1	1.68	26		39.3	1.59
8		36.5	1.56	27		37.1	1.57
9		35.0	1.54	28		55.3	1.74
10		28.1	1.45	29		41.1	1.61
11		31.2	1.49	30		36.3	1.56
12		33.2	1.52	31		50.5	1.70
13		29.0	1.46	32		47.2	1.67
14		32.2	1.51	33		45.1	1.65

Compound ID	R	% Inhibition	log %	Compound ID	R	% Inhibition	log %
15		39.3	1.59	34		53.0	1.72
16		33.2	1.52	35		67.5	1.83
17		39.3	1.59	36		71.2	1.85
18		44.1	1.64	Ibuprofen		40.2	1.60
19		40.2	1.60	Diclofenac		52.4	1.72

3. 1. QSAR Analysis of N³ Substituted 5,7-dimethyl-3H-thiazolo[4,5-b]pyridin-2-one derivatives

The structures of thiazolo[4,5-*b*]pyridin-2-ones under study were subjected to energy minimization with MM+ force field followed by the repeated minimization with semi-empirical AM1 method. Molecular descriptors for 3D optimized structures of the compounds were calculated with E-DRAGON software. Descriptors with the constant and near constant values were discarded. Descriptors with high pairwise correlation, determined based on correlation matrix analysis, were excluded from the multidimensional descriptor space. As a result, the set of 482 descriptors was obtained for both training and test sets compounds. The descriptor normalization procedure was carried out, the values of all generated descriptors were scaled in the range of 0÷1.

Activity sampling method was used for splitting overall dataset into the training and validation (test) sets. The main steps of the technique included sorting compounds by activity. Then the size of a group of compounds was specified by including the specified number of the most active compounds into the first group, the same number of the next most active compounds into the second group, etc. Then the number of compounds in each

group, which would be included into the training and test sets, was determined. Thus, all compounds were divided into 6 groups, the numbers of compounds with low, moderate, and high levels of activity in each group were approximately the same. Then a few compounds from each group were assigned to the validation set, and the rest compounds formed the training set. The results of the dataset splitting are given in Table 2.

The selection of the optimal set of molecular descriptors was carried out using genetic algorithm within each of descriptors' modules namely 0D-, 1D-, 2D, 3D and module "Other" firstly. The most significant descriptors from each dimensionality module were introduced to the final data set. Multiple Linear Regression (MLR) was used to generate QSAR models as a multivariate linear regression within the training set compounds with BuiltQSAR software.

Among the generated models 1 one-parameter and 2 two-parameter QSAR models were selected with the highest statistical characteristics and predictive ability:

$$\log \% = -0.3423 \text{ GATS7m} + 1.8669 \quad (\text{Model 1});$$

$$\log \% = 0.1315 \text{ MATS4e} - 0.2781 \text{ GATS7m} + 1.7706 \quad (\text{Model 2});$$

$$\log \% = 0.1318 \text{ MATS4m} - 0.2998 \text{ GATS7m} + 1.7961 \quad (\text{Model 3}).$$

Table 2. The number of compounds in training and test sets constructed by the ranking of compounds activities

Group number	Size of a group	Number of compounds assigned to the training set	Compounds ID	
			Training set	Test set
I	6	4	1, 28, 34, 36	2, 35
II	5	4	5, 6, 31, 32	7
III	7	5	4, 18, 20, 24, 33	25, 3
IV	6	5	17, 19, 21, 26, 29	15
V	6	5	8, 9, 23, 27, 30	22
VI	6	4	10, 11, 12, 14	13, 16

Models 1–3 were constructed using 2D autocorrelation descriptors GATS7m (Geary autocorrelation of lag 7 weighted by mass), MATS4e and MATS4m (Moran autocorrelations of lag 4 weighted by atomic Sanderson electronegativity and by mass, respectively) with low pairwise correlation. The normalized values of molecular descriptors for both training and test sets compounds are listed in Table 1S of the Supplementary materials. To ensure the accuracy in predicting ability of the generated models, the prediction errors and the prediction error standard deviations were calculated (Table 2S of the Supplementary materials).

Based on the validation parameters of the generated models (Table 3), all constructed models satisfied the statistical requirements for their goodness-of-fitting with no current overfitting. Goodness of fitting for QSAR models generated with p parameters for the training set consisting of 27 compounds was assured by maximizing the correlation coefficient R and the determination coefficient R^2 , adjusted regression coefficient R^2_{adj} and F -test criterion while minimizing $R^2 - R^2_{adj}$ and standard deviation s .

Pearson correlation coefficient R measures the strength of the linear relationship between dependent and independent variables with possible values between -1 and 1. In regression, R -squared (R^2 , or the coefficient of determination) is a statistical measure of how well the regression predictions approximate the real data points providing the relative measure of the percentage of the dependent variable variance that the model explains. The higher val-

Table 3. Statistical parameters for QSAR models 1 – 3

No	Statistical parameter	Model 1	Model 2	Model 3
1.	p	1	2	2
2.	R	0.8117	0.8772	0.8728
3.	R^2	0.6589	0.7694	0.7617
4.	R^2_{adj}	0.6452	0.7502	0.7419
5.	$R^2 - R^2_{adj}$	0.0137	0.0192	0.0198
6.	s	0.0534	0.0448	0.0455
7.	F	48.2900	40.0412	38.3644
8.	p	0	0	0
9.	$DF_{regression}$	1	2	2
10.	SSR	0.1377	0.1608	0.1592
11.	MSR	0.1377	0.0804	0.0796

ues of R^2 indicates the high fitness of the model as R^2 of 1 indicates that the regression predictions perfectly fit the data. Adjusted R -squared R^2_{adj} considers and tests different independent variables against the model. Its value may increase or decrease depending on the significance of the independent variable introduced to the regression. So, the higher value of R^2_{adj} ensures the high significance of all variables introduced into the model. The standard deviation (s) is a measure of the amount of variation or dispersion of a set of values. A low standard deviation indicates that the values tend to be close to the mean (also called the expected value) of the set. The F -test reflects the ratio of the variance explained by the model and the variance due to the error in the regression. High values of the F -test indicate that the model is statistically significant.

The degree of freedom for the regression equals to the number of independent parameters: $DF_{regression} = p$. It defines the number of values is a dataset having the freedom to vary. $SS_{regression}$ (SSR) means the **Sum of squares** for the regression while $MS_{regression}$ (MSR) means the **Mean square** for the regression. Regression sum of squares is interpreted as the amount of total variation that is explained by the model. SSR is variation in Y_i associated with the regression line, \bar{Y} . It may be referred to as the measure that describes how well our line fits the data. $MS_{regression}$ is

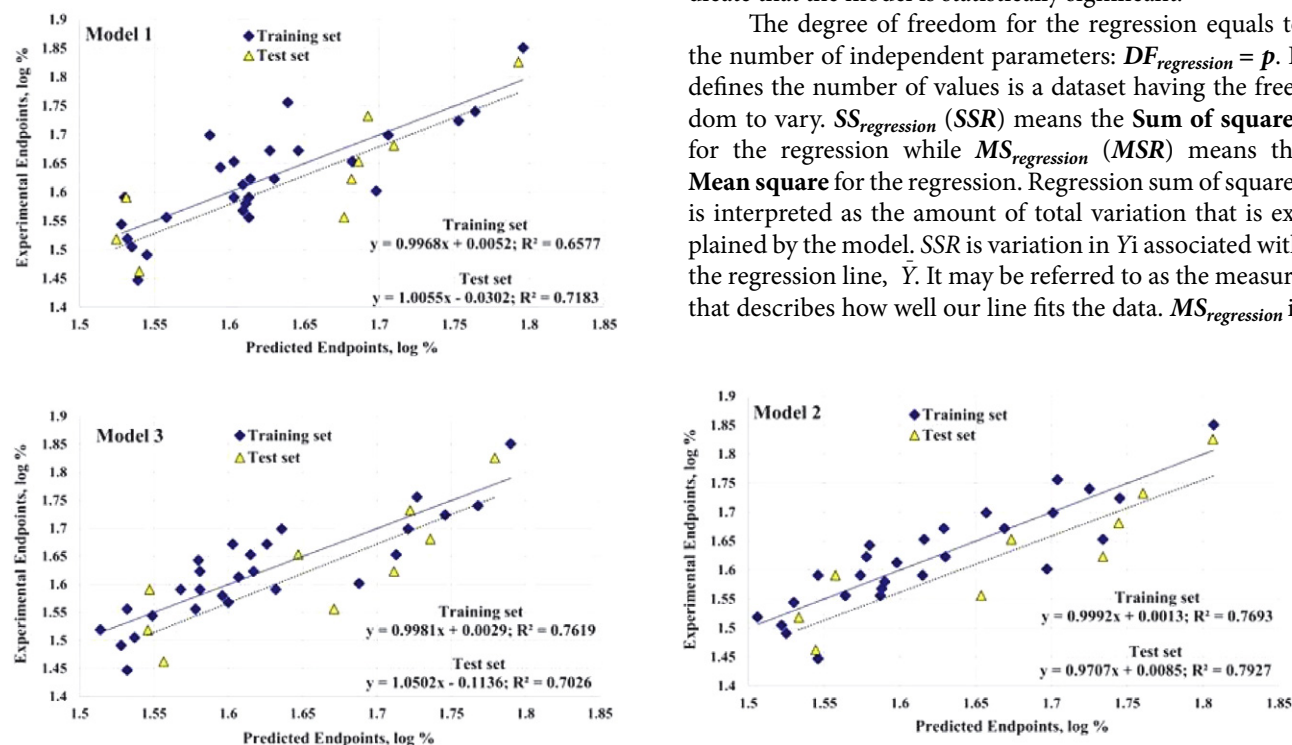


Fig. 2. Correlation between observed activity and activity predicted with Models 1 – 3 together with linear fit statistical parameters

an estimate of the variance of regression, $MS_{\text{regression}} = SS_{\text{regression}} / DF_{\text{regression}}$.

Thus generated QSAR models could approximate the experimental values properly according to their statistical analysis performance parameters.

Predictive ability of the generated models was ensured by using leave-one-out (LOO) cross-validation procedure, when each object is removed from the original training dataset once in turn and the remaining reduced data set is converted into new training set used for a model generation and the response prediction for the excluded compound. The outcome from this procedure is leave-one-out cross-validation coefficient Q^2_{LOO} . The coefficients of determination between observed and predicted activities $R^2_{\text{(observed vs. predicted)}}$ for the training set compounds were also estimated as an internal validation predictivity. Figure 2 shows the regression lines between experimental anti-exudative activity and activity predicted with Models 1-3.

The determination coefficients for observed end-points versus experimental one for the derived models were in the range between 0.6577 and 0.7693, so the linear models explained 65.77% – 76.93% of variation in experimental activity. We evaluated the accuracies of QSAR models also using the difference $|R^2 - Q^2_{\text{LOO}}|$ absolute value supposing that it tends to minimum for truly predictive model.

The values of Q^2_{LOO} (0.6025 ÷ 0.6995) were reasonable, showing that the models were significant and robust to predict the anti-exudative activity of the compounds under study. We also considered that the values of the difference between R^2 and Q^2_{LOO} ($|R^2 - Q^2_{\text{LOO}}|$) were within the suggested limit of $|R^2 - Q^2_{\text{LOO}}| < 0.3$,⁴³ which was the indication that the models had no data overfitting. S_{PRESS} is the predicted residual sums of squares standard deviation, and S_{DEP} is the standard deviation error in prediction. Internal validation parameters are summarized in Table 4.

Table 4. Internal validation parameters for QSAR models 1 – 3

No	Validation parameter	Model 1	Model 2	Model 3
1.	$R^2_{\text{(observed vs. predicted)}}$	0.6577	0.7693	0.7619
2.	Q^2_{LOO}	0.6025	0.6995	0.6908
3.	$ R^2 - Q^2_{\text{LOO}} $	0.0552	0.0698	0.0711
4.	S_{Press}	0.0576	0.0512	0.0519
5.	S_{DEP}	0.0565	0.0491	0.0519
7.	DF_{error}	25	24	24
8.	SSE	0.0713	0.0482	0.0498
9.	MSE	0.0029	0.0020	0.0021

For internal validation we also applied S_{DEP} (standard deviation of error of predictions), which makes a distinguish between ‘predictions’ for new data points which

were not involved into the model construction, and the standard deviation of the predicted residual error sum of squares S_{PRESS} . S_{PRESS} is a form of cross-validation used in regression analysis to provide a summary measure of the fit of a model to a sample of observations that were not themselves used to estimate the model. Both S_{PRESS} and S_{DEP} values display tendency to minimization to ensure that generated models possessed enough predictive power. We also applied SSE as the **Sum of squares error** and MSE as the **Mean square error**. MSE measures error in statistical models by using the average squared difference between observed and predicted values. Highly predictive linear regression should display minimized SSE . The degree of freedom for residuals (errors) equals: $DF_{\text{error}} = n - p - 1$, where n is the number of observations in the training set. MSE is an estimate of the variance of errors: $MSE = SSR / DF_{\text{error}}$. If the regression model is “perfect”, SSE is zero. Thus, MSE is a measure of the quality of an estimator. As it is derived from the square of Euclidean distance, it is always a positive value that decreases as the error approaches zero.

To estimate the predictive power of QSAR models, we employed the test set compounds for their external validation. The following statistical characteristics are recommended:^{44,45} (i) Q^2_{LGO} ; (ii) coefficient of determination R^2_{ext} between the predicted and observed activities; (iii) coefficients of determination (predicted versus observed activities, and observed versus predicted activities) for regressions through the origin; (iv) slopes k and k' of the regression lines through the origin. For acceptable QSAR predictive models, they should satisfy the following conditions:

- (i) $Q^2_{\text{LGO}} > 0.5$; (ii) $R^2_{\text{ext}} > 0.6$; (iii) $(R^2_{\text{ext}} - R^2_{0\text{ext}}) / R^2_{\text{ext}} < 0.1$ and $0.85 \leq k \leq 1.15$ or $(R^2_{\text{ext}} - R^2_{0\text{ext}}) / R^2_{\text{ext}} < 0.1$ and $0.85 \leq k' \leq 1.15$; (iv) $|R^2 - R^2_{0\text{ext}}| < 0.1$.

The values of the external validation criteria are summarized in Table 5.

Table 5. External validation criteria values for Models 1 – 3

No.	Validation criteria	Model 1	Model 2	Model 3
(i)	Q^2_{LGO}	0.6790	0.9860	0.6211
(ii)	R^2_{ext}	0.7183	0.7927	0.7026
(iii)	$R^2_{0\text{ext}}$	0.9988	0.9991	0.9988
	$(R^2_{\text{ext}} - R^2_{0\text{ext}}) / R^2_{\text{ext}}$	-0.3905	-0.2604	-0.4216
	k	1.0118	1.0239	1.0172
	k'	0.9872	0.9758	0.9818
(iv)	$ R^2 - R^2_{0\text{ext}} $	0.2805	0.2064	0.2962

Based on the statistical evaluation and predictive power of the developed models, it may be concluded that Model 2 is the most reliable with the highest good-

ness-of-fitting assuring, statistical significance, robustness and externally predictivity.

A mechanistic interpretation for a generated QSAR models was then done to make the interpretation of the possible mechanism of activity. All constructed models contain 2D autocorrelation descriptors. In particular, all models contain Geary autocorrelation coefficients with lag 7, weighted by atomic masses (**GATS7m**). Models **2** and **3** contain Moran autocorrelations of lag 4 weighted by atomic Sanderson electronegativity and by mass (**MATS4e** and **MATS4m**, respectively). In general, 2D autocorrelation descriptors represent the topological structure of compounds, describe the mutual correlation of certain properties of atoms in intervals equal to the sums of topological distances in the corresponding structural fragments. They are calculated from molecular graph G by summing the products of atom weights of the terminal atoms of all the paths of the considered path length (the lag). 2D autocorrelation descriptors are calculated based on the value of the autocorrelation function $ATS(d)$.^{46,47}

$$ATS(d) = \sum_{i=1}^A \sum_{j=1}^A \delta_{ij} \cdot (\omega_i \cdot \omega_j)_d \quad (7)$$

where d is the corresponding lag, or the number of topological distances in a single fragment of the molecular graph, can have the values between 1 and the maximal topological distance in the molecule; A is the number of atoms in the molecule;

$\delta_{ij} = \begin{cases} 0 & (d_i \neq d) \\ 1 & (d_i = 0) \end{cases}$ – Kronecker's delta; ω_i, ω_j – physicochemical properties of the atoms i and j (atomic masses m , polarizability p , electronegativity e , van-der-Waals volume v).

The Moran autocorrelation descriptors ($MATS_{dw}$) are given by:

$$I(d) = \frac{\frac{1}{\Delta} \sum_{i=1}^A \sum_{j=1}^A \delta_{ij} (\omega_i - \bar{\omega}) (\omega_j - \bar{\omega})}{\frac{1}{A} \sum_{i=1}^A (\omega_i - \bar{\omega})^2} \quad (8)$$

where $\bar{\omega}$ is the average value of the property for the molecule, and $\Delta = \sum \delta_{ij}$ is the number of vertex pairs at distance equal to d . The computation of these descriptors involves summing different autocorrelation functions corresponding to different fragment lengths, thereby leading to different autocorrelation vectors according to the lengths of the structural fragments. Also, weighting components in terms of physicochemical properties has been considered, and therefore these descriptors address the topology of the structure or parts of its merged with a selected physicochemical property. Moran autocorrelations usually have values in the interval of $[-1, +1]$ with the positive autocorrelations corresponding to positive values of Moran indices, while the negative autocorrelations correspond to negative values of these indices.

The Geary autocorrelation descriptors ($GATS_{dw}$) are given by:

$$C(d) = \frac{\frac{1}{2\Delta} \cdot \sum_{i=1}^A \sum_{j=1}^A \delta_{ij} \cdot (\omega_i - \omega_j)^2}{\frac{1}{(A-1)} \cdot \sum_{i=1}^A (\omega_i - \bar{\omega})^2} \quad (9)$$

2D Geary autocorrelation coefficients are the functions of distances and may vary between 0 and ∞ . At the same time, strong mutual correlations of atomic properties correspond to low values of the Geary autocorrelation, usually in the range between 0 and 1, while negative mutual correlations correspond to values of the Geary coefficient higher than 1, i.e., the statement "no autocorrelation" corresponds to the equality $C(d) = 1$.

The presence of lags 4 2D Autocorrelations in QSAR regressions **2** and **3** may be reviewed as the association of activity information content with structural fragments of such size. It should be noted that mass weighted Moran autocorrelation coefficient **MATS4m** made a positive contribution to the activity. Based on these models' interpretation, it can be stated that the presence of structural fragments with the sum of topological distances (lag) equal to 4 in the molecules of the training set substances, whose terminal atoms have high atomic masses and electronegativities, corresponds to the activity enhancing. All generated regressions also utilize 2D Geary autocorrelation **GATS7m** descriptor with the negatively signed regression coefficients. Based on the interpretation and analysis of Geary autocorrelations contribution into anti-exudative activity it can be asserted that the presence of structural fragments with sums of topological distances (lags) equal to 7, whose terminal atoms have high atomic masses, is undesirable. The possible structural fragments with lags 4 and 7 are depicted in Figure 3.

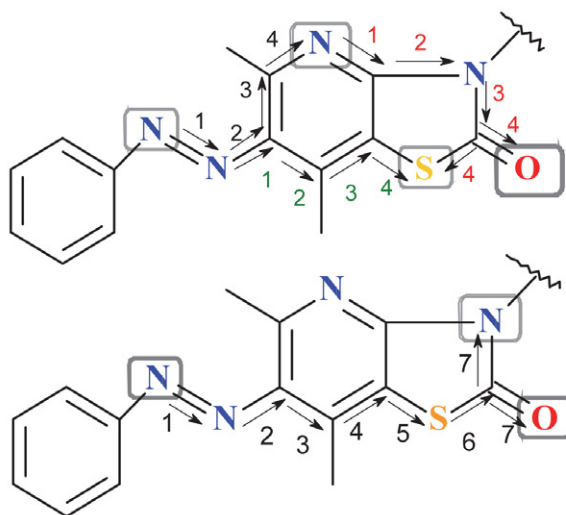


Fig. 3. Possible structural fragments with lags 4 and 7 in the molecules of N^3 substituted 5,7-dimethyl-6-phenylazo-3H-thiazolo[4,5-b]pyridin-2-one derivatives which may contribute to their anti-exudative action mechanism

It may be concluded that small structural patterns which include heteroatoms of fused thiazole and pyridine

core, and also one of the azo-group nitrogen atoms and closest scaffold heteroatom, may contribute mutually to the anti-exudative action mechanism, while the presence of large motifs started with azo-group nitrogen and ending at oxygen or nitrogen atoms of thiazolidin-2-one, cannot be involved into the activity mechanism realization.

3. 2. Molecular Docking

Suppression of prostaglandin synthesis is associated with inhibition of cyclooxygenase enzyme activity that catalyses the deoxygenation of arachidonic acid (AA) to form prostaglandin G₂ (PGG₂), then prostaglandin H₂ (PGH₂), and finally the resultant prostaglandins and thromboxane A₂ (TxA₂).⁴⁸ The mechanism of traditional non-steroidal anti-inflammatory drugs (NSAIDs) action is based on non-selective inhibition of both cyclooxygenase isoforms (COX-1 and COX-2) and preventing prostaglandin synthesis. It is supposed that the therapeutic effect of these substances is due to the inhibition of COX-2, but their effect on COX-1 causes damage to the mucous membrane of the gastrointestinal (GI) tract and disorders in regulation of renal and platelet activity.⁴⁹ Selective COX-2 inhibitors (coxibs) inhibit the COX-2 isoform while spare COX-1 at clinical doses. This greatly mitigates the adverse effects in the GI tract as well as bleeding secondary to diminished platelet function.⁵⁰ Additional importance of COX-2 specific drugs discovering relates to their broader therapeutic applications as the biological role of COX-2 extends beyond inflammation and pain. It is known that COX-2 plays a key role in early female reproductive function, implantation and decidualization are dependent on COX-2.⁵¹ Recent reports suggest that COX-2 may be an effective antitumor therapeutic target as COX-2 overexpression has been reported in several human cancers including lung, colon, prostate, and bladder cancer.^{52–54} Selective COX-2 inhibitors, although characterized by a much lower negative effect on the digestive system, also have undesirable side effects, in particular, their effect on the cardiovascular system increases the risk of myocardial infarction, heart failure, stroke, etc.⁵⁵ In the light of these complications, it was proposed to identify other drug targets downstream of COX for pain and inflammation therapy. One of the promising new targets for finding bioactive substances that exhibits anti-inflammatory effect is microsomal prostaglandin E synthase-1 (mPGES-1) – the final enzyme in the cascade of arachidonic acid transformations. mPGES-1 is able to convert the cyclooxygenase (COX)-derived unstable prostaglandin H₂ (PGH₂) to the bioactive prostaglandin E₂ (PGE₂).⁵⁶ mPGES-1 belongs to a superfamily of Membrane-Associated Proteins (MAPEG family), involved into Eicosanoid and Glutathione metabolism, therefore it is useful for the development of anti-inflammatory and anticancer drugs interfering with prostaglandin and leukotriene biosynthesis.⁵⁷ mPGES-1 is regarded as a promising target for selectively suppressing

PGE₂ production during inflammation and nociceptive processing owing to its preferential coupling with COX-2.⁵⁸ But, contrary to the classical non-steroidal anti-inflammatory drugs (NSAIDs), the inhibition of mPGES-1 does not affect the biosynthesis of the other physiologically important PGs.⁵⁹ Possible mechanisms of mPGES-1 inhibitors activity are competitive interaction with active centres of cofactor or substrate. Inhibition of mPGES-1 has been shown to result in systemic shunting of PGH₂ to PGI₂ formation, leading to anti-inflammatory and vasodilatory effects, while preventing platelet activation.⁶⁰

We utilized the standard MOE-Dock architecture for the molecular docking studies of N³ substituted 5,7-dimethyl-6-phenylazo-3H-thiazolo[4,5-*b*]pyridin-2-ones with the selected receptors included the following major components: ligand conformations generation followed by partial charges calculation and energy minimization, receptors preparation, the binding sites definition, the ligand-receptor pose generation with alpha triangle as the placement algorithm, docking and scoring proceeding, receptor-ligand complexes refinement with re-scoring by filtering queries application, the lowest energy complexes extraction with the resulting complexes minimization. A data set of 2545 conformations for 36 compounds under study was prepared in this way. Docking poses were produced from the placement and the minimized receptor-ligand complexes obtained were then scored by the four scoring functions available in MOE: Affinity dG, Alpha HB, London dG, and GBVI/WSA dG Scorings.

3.2.1. Docking Results with COX-1 and COX-2

Both COX-1 and COX-2 isoforms are dimers consisting of 576 and 581 amino acids, respectively, while both iso-enzymes share the same molecular mass of 70 kDa/monomer. Each COX monomer consists of three structural domains:⁶¹ a short N-terminal epidermal growth factor domain, a membrane binding domain, and a large, globular C-terminal catalytic domain. The cyclooxygenase and peroxidase active sites are located on opposite sides of the catalytic domain with inhibitor bound only in the cyclooxygenase active site. COX-1 and COX-2 isoforms present a high degree of homology.⁶² The entrance to the COX active site occurs at the base of the membrane binding domain and leads to a long hydrophobic channel that extends deep into the interior of the catalytic domain.⁶³ The COX channel is composed of three residues (Arg-120, Tyr-355, and Glu-524) that separates the channel from the active site. The hydrophobic catalytic pocket contains catalytic Tyr-385 as well as Ser-530 at the top of the pocket, and also Trp-387, Phe-518, Ala-201, Tyr-248 and Leu-352. The COX-1 and COX-2 active sites are very similar but differ in the presence of a side pocket with larger solvent accessible surface in COX-2 located above the Arg-120/Tyr-355/Glu-524 constriction. This COX-2 side pocket is bordered by Val-523 (Ile-523 in COX-1) and contains His-90 and a

conserved Arg-513 (His-513 in most COX-1) at the base of the side pocket.⁶⁴ Most NSAIDs act inhibiting non-selectively both COX-1 and COX-2 iso-enzymes in a competitively reversible noncovalent manner. Aspirin is the only clinically used inhibitor modifies covalently and irreversibly both COX-1 and COX-2 through acetylation of Ser-530.⁶⁵ Aspirin analogues, like 2-bromoacetoxybenzoic acid and *o*-acetylsalicylhydroxamic acid, also bind in the COX-1 active site channel, acetylate Ser-530, and hydrogen-bond with Arg-120 at the constriction of the site.⁶⁶ In the existing crystal structures of COX with aspirin analogues, a hydrogen bond is formed between the carbonyl

oxygen of the acetyl adduct and the phenolic hydrogen of Tyr-385, thus the presence of Tyr-385 across the active site from Ser-530 appears to be a critical determinant of acetylation.⁶⁷ Phenylpropionic and arylacetic acid inhibitors (naproxen, diclofenac, indomethacin, ibuprofen, flurbiprofen, mefenamic acid, and meclofenamic acid) form a two-step binding mode for COX inhibition forming an ion pair and/or hydrogen bond with Arg-120 (this interaction is critical for inhibition) and a hydrogen bond with Tyr-355.⁶⁸ The unique binding mode of diclofenac with COX-2 is based on its inverted binding with the carboxylic acid moiety *via* hydrogen-bonded to Ser-530 and Tyr-385. The

Table 6. Calculated docking scores for 36 N³ substituted 5,7-dimethyl-6-phenylazo-3*H*-thiazolo[4,5-*b*]pyridin-2-one derivatives in complexes with COX-1 and COX-2

Compound ID	COX-1				COX-2			
	GBVI/WSA dG	London dG	Alpha HB	Affinity dG	GBVI/WSA dG	London dG	Alpha HB	Affinity dG
1	-3.5721	-8.9854	-102.5757	-4.5784	-4.7093	-11.2232	-75.6134	-4.0763
2	-3.4101	-10.2535	-88.3039	-5.6864	-0.5564	-12.4995	-74.2815	-4.9970
3	-3.5094	-10.1962	-86.8319	-5.7342	-2.0131	-12.8897	-78.0022	-6.4081
4	-2.0678	-9.9628	-107.7880	-6.7700	-2.0915	-11.6763	-76.0573	-4.6654
5	-3.6256	-8.1085	-87.9495	-5.4172	-2.4295	-11.9037	-75.1318	-4.7097
6	-2.0591	-10.1058	-108.9735	-7.3861	-5.0659	-12.7828	-90.2685	-7.1683
7	-2.1836	-10.1408	-118.3711	-7.3602	-5.0118	-12.7031	-78.0846	-6.5735
8	-3.5894	-9.0593	-86.7782	-5.7160	-0.5586	-12.0557	-65.6218	-5.1219
9	-3.3979	-9.8344	-135.8003	-7.8005	-5.5785	-13.8054	-83.1410	-6.8872
10	-3.9388	-10.5867	-144.8922	-8.6517	-4.9257	-14.6358	-93.0085	-7.5152
11	-3.8215	-8.9786	-135.7580	-8.4577	-6.2059	-15.1357	-85.5426	-8.2501
12	-3.8334	-9.8577	-129.3662	-8.4110	-5.7290	-14.7253	-86.3963	-7.7120
13	-3.7142	-12.4254	-129.5875	-7.8616	-4.1096	-13.8382	-78.8016	-7.4252
14	-4.3321	-10.3371	-155.4785	-8.1072	-5.7120	-15.0507	-79.7068	-7.9452
15	-2.4523	-11.0348	-136.3768	-7.3664	-5.7441	-14.0444	-80.4431	-7.0865
16	-3.3274	-11.6665	-143.5742	-6.9413	-5.6076	-14.0993	-86.9043	-7.1747
17	-3.9379	-11.9141	-129.8906	-8.0258	-4.7478	-14.1567	-84.6444	-8.3579
18	-2.3838	-10.2205	-124.5617	-6.8422	-3.6734	-11.9241	-78.3305	-4.6454
19	-1.2252	-9.0904	-132.0742	-4.9922	-4.7933	-13.8596	-94.6653	-5.1191
20	-2.6893	-14.1219	-135.4255	-8.8465	-4.6539	-16.0134	-64.9250	-9.7737
21	-2.6710	-13.1721	-132.7236	-8.1597	-5.2945	-17.3721	-98.9472	-8.8459
22	-4.4923	-10.5589	-137.0937	-8.4308	-5.4785	-13.4701	-89.1642	-5.8359
23	-2.3580	-12.8478	-172.6101	-8.5650	-3.9622	-15.0712	-87.9949	-6.0371
24	-2.2812	-10.5789	-137.5367	-8.1755	-4.1854	-16.2461	-87.2868	-8.1194
25	-2.8548	-10.7060	-132.2015	-7.8614	-4.3432	-14.3780	-81.6798	-7.8906
26	-3.7227	-12.1064	-128.3981	-8.0519	-5.2332	-16.7522	-96.1670	-8.7652
27	-3.4848	-8.9993	-144.0276	-7.9182	-4.6807	-18.3361	-97.7554	-8.6181
28	0.1975	-11.4950	-126.1505	-6.7385	-6.0431	-14.7884	-76.8276	-6.6816
29	-6.7684	-12.0197	-140.5306	-5.6753	-7.1984	-16.2490	-84.0470	-8.4898
30	-2.8618	-11.1192	-186.8507	-8.2221	-5.1307	-17.3107	-108.0430	-8.6079
31	-2.8262	-8.7345	-149.1720	-7.4661	-2.2133	-16.3997	-89.4604	-8.0642
32	-7.6292	-11.5782	-151.1346	-9.9868	-5.7125	-18.2977	-93.5176	-10.1135
33	-0.6069	-11.8933	-127.6375	-6.3678	-6.6209	-14.8906	-90.3635	-8.3991
34	1.6951	-12.7936	-177.5706	-9.8437	-7.0093	-16.0785	-107.9989	-10.7538
35	-4.0370	-3.9965	-135.4871	-9.4130	-3.4646	-17.2437	-85.9848	-8.6887
36	-5.0688	-7.1341	-155.8307	-8.3196	-4.0012	-19.3118	-97.8379	-10.0296
Diclofenac	-0.6979	-10.5624	-95.7075	-6.0407	-3.9428	-9.2298	-107.4595	-7.3823
Naproxen	-	-	-	-	-7.2959	-13.9041	-94.5634	-6.0959
α-methyl-4-biphenyl-acetic acid	-7.6663	-13.9861	-102.8187	-7.7516	-	-	-	-

inhibitor also forms extensive van der Waals interactions with several hydrophobic residues within the active site. Indomethacin binds deeply within the COX-2 active site with its *p*-chlorobenzoyl group projects up into the active site channel, and the chlorine atom interacts with Leu-384 at the top of the active site, while the benzoyl oxygen interacts with Ser-530. The benzoyl group itself is stabilized by hydrophobic interactions with Leu-384, Tyr-385, Phe-381, and Trp-387. The carboxylate of indomethacin forms a salt bridge with Arg-120 and makes additional contacts with Tyr-355. The *o*-methoxy group protrudes into a large cavity provided by Ser-353, Tyr-355, and Val-523. The indole ring interacts with Val-349 and the 2'-methyl group projects into a small hydrophobic pocket formed by Val-349, Ala-527, Ser-530, and Leu-531, this interaction is supposed as a key interaction responsible for the time-dependent inhibition of COX enzymes by this inhibitor.⁶⁹ When turning to COX-2 selective inhibitors, it was shown, for instance, that lumiracoxib also binds in the COX-2 active site in an inverted orientation: its carboxylate forms hydrogen-bonding interactions with Ser-530 and Tyr-385 at the top of the active site, similar to diclofenac while the methyl group on the phenylacetic acid ring projects into a small groove near Leu-384 in the COX-2 active site. For diaryl heterocycle class of COX-2 selective inhibitors (celecoxib, rofecoxib, valdecoxib, etoricoxib) structure-activity analysis revealed that the fundamental factors responsible for the potent and selective inhibition of COX-2 include (1) two aromatic rings on adjacent positions on a central scaffold and (2) the presence of a sulfonamide or methyl sulfone group on one of the phenyl rings.

Docking calculations for N³ substituted 5,7-dimethyl-6-phenylazo-3*H*-thiazolo[4,5-*b*]pyridin-2-ones were performed considering the X-ray crystallographic data of oCOX-1 and mCOX-2 with high resolutions downloaded from PDB (PDB entry codes 1Q4G, 3NT1 respectively). The most probable binding sites within the macromolecules were detected by means of MOE Site Finder, the alpha triangle as the placement algorithm was selected, running by superposition of ligand atom triplets and triplets of receptor site points. The receptor site points were represented by alpha sphere centres. At each iteration, a random ligand conformation was selected. A random triplet of ligand atoms and a random triplet of alpha sphere centres were used to determine the pose. The following docking calculations were performed by means of the DOCK tool implemented in MOE with the first rescoring function setting as "London dG", and the obtained poses were refined and rescored based on the refinement scoring function fixing to "GBVI/WSA dG". The values of the calculated docking scores for the compounds under study in their complexes with COX-1,2 are listed in Table 6. Also, co-crystallized ligands (α -methyl-4-biphenylacetic acid in case of COX-1 and naproxen for COX-2) and diclofenac were docked to the receptors as references.

The calculated values of the docking scores for the most energetically favourable receptor-ligand complexes suggest the possible inhibitory activity of 3*H*-thiazolo[4,5-*b*]pyridin-2-ones against both COX iso-forms expressed non-selectively. Alpha HB Scoring as a measure the geometric fit of the ligand to the binding site and hydrogen bonding effects, has significantly higher negative values for ligand-COX-1 complexes in comparison with the ligands complexed with COX-2 including reference drugs. Affinity dG Scoring, which estimated the enthalpic contribution to the free energy of binding, are comparable for both COX-1 and COX-2 complexes with a corresponding ligand.

In case of COX-1 complexes, the values of London dG Scoring, which estimates the free energy of binding of the ligand from a given pose, are close in values to that one for diclofenac while London dG Scoring for α -methyl-4-biphenylacetic acid-COX-1 complex has higher negative value. In case of ligands-COX-2 complexes London dG Scoring is comparable with that one for naproxen-COX-2 complex and has considerably higher negative values as compared with the corresponding ligand-COX-1 and diclofenac-COX-2 complexes, indicating higher thermodynamic probability of inhibitory activity towards COX-2 isoform.

We further analysed the detailed binding modes for COX-1,2 complexes with ligands keeping in mind that the compounds under study starting from **9** contain bulky substituents in their N³ position and phenyl-azo group in C⁶ position while they have no carboxylic group for catalytic Tyr-385 H-binding or Ser-530 acetylation.

It is well known that arylacetic acid inhibitors while binding to COX-1 and COX-2 active sites show two different binding modes with their acidic groups position either coordinating to the catalytic Tyr-385 as well as Ser-530 at the apex of the pocket or to the constriction residues Arg-120 and Tyr-355 at the base of the active site. α -Methyl-4-biphenylacetic acid, the defluorinated analogue of flurbiprofen, binds to COX-1 at the entrance of the long channel which leads into the enzyme active site, forming H-bonding interactions with Arg-120 and Tyr-355. Binding at this site presumably blocks access of substrate to Tyr-385, a residue essential for catalysis.³⁸ Similarly, the X-ray crystallographic structure of COX-2 in complex with naproxen³⁹ adopts that naproxen is bound entirely within the main channel of the COX-2 active site in the opposite binding mode: the carboxylate group of naproxen participating in hydrogen-bonding interactions with Arg-120 (2.8 Å) and Tyr-355 (2.5 Å) at the base of the active site while *p*-methoxy group is oriented toward the top of the hydrophobic channel. The remainder of the interactions between the compound and protein are van der Waals contacts.

The inspected binding modes of 5,7-dimethyl-6-phenylazo-3*H*-thiazolo[4,5-*b*]pyridin-2-ones within COX-1,2 active sites revealed that two main ligands orientations are

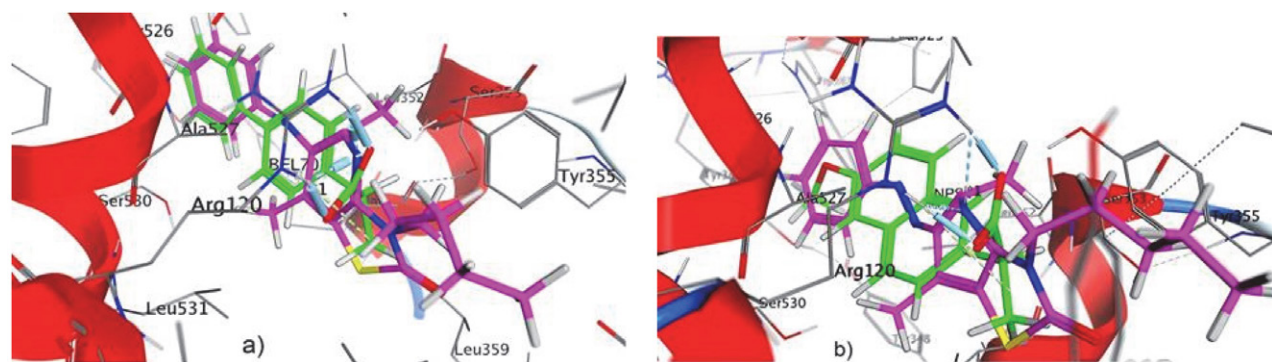


Fig. 4. Three-dimensional binding models of compound **6** in the active sites of COX-1 and COX-2: a) Compound **6** (magenta) overlaid with co-crystallized 2-(1,1'-biphenyl-4-yl)propanoic acid (green) in COX-1 active site; b) Compound **6** (magenta) overlaid with co-crystallized naproxen (green) in COX-2 active site

possible: the N³ position substituent may be directed both inside and outside of the hydrophobic binding channel of the receptor. Figure 4 shows the binding modes of compound **6** with COX-1 and COX-2.

The binding orientations and interaction mechanisms in ligand-COX-1,2 complexes for the most active compounds are shown in Table 7.

The majority of top ranked poses of N³ substituted thiazolo[4,5-*b*]pyridin-2-one derivatives docked into COX-1 active site are oriented with their phenylazo group directed inside the hydrophobic pocket with the complex formation maintaining on account of mainly Nitrogen of pyridine core hydrogen-bonding interaction with Arg-120. In some complexes additional stabilization on account of π -cation interaction between thiazole ring and Arg-120 (compounds **4**, **7**, **15**, **16**, **18**, **25**, **26**, **30** and **31**), also H-binding of Oxygen of N³-substituent acetamide moiety with Arg-120 and Tyr-355 amino acid residues (compounds **14**, **20**). Also compound **20** has been shown to make π -H interaction of phenyl moiety of the substituent with Ile-89 which is thought to be one of the important residues in the lobby region of the protein active site. H-binding between Nitrogen of phenylazo group and Arg-120 is preferable for compounds **1**, **2**, **3**, **5**, **8** and **21** in their complexes with COX-1. In compound **2** - COX-1 complex Nitrogen of nitrile group forms additional binding with Arg-120. Additional hydrogen bond between Oxygen of thiazolidine ring and Arg-83 is forming for compounds **3**, **5**, **8**, **21**. Oxygen of acetamide moiety is forming hydrogen-bonding interactions with both Arg-120 and Tyr-355 for docking poses of compounds **19**, **23**, **24**, **34** in COX-1 active site. The same binding between Oxygen of acetamide moiety with both Arg-120 and Tyr-355 is observed for compound **34** while the ligand in this case has the opposite orientation with the N³ position substituent orient towards the apex of the catalytic pocket. The same ligand orientation is displayed by compound **36** while the binding with COX-1 in this case is achieved *via* H-bonds between Nitrogen of methylene amino moiety of the substituent and Arg-120, Nitrogen of phenylazo group and

Arg-83 and additional π -H interaction between pyridine ring and Ile-89.

Similarly, the majority of top ranking poses of N³ substituted thiazolo[4,5-*b*]pyridin-2-ones docked into COX-2 active sites show that phenylazo group is directed inside the hydrophobic pocket with the complex formation maintaining on account of mainly Nitrogen of pyridine core hydrogen-bonding interactions with Arg-120 or Tyr-355, located at the base of the active site. Some compounds bind deeply with COX-2 active site forming hydrogen bonds between Oxygen of N³-substituent acetamide moiety and Arg-120 amino acid residue as a single binding (compounds **20**, **22**, **24**, **26**, **27**, **30**) or in combination with N of pyridine cycle – Tyr-355 H-binding (compounds **10**, **11**, **28**). Additional complexes stabilization may be achieved on account of π -cation interaction between thiazole ring and Arg-120 or π -H interaction between pyridine ring and Tyr-355. While for a few derivatives the opposite orientation in COX-2 active site with the N³ position substituent orientation towards the apex of the catalytic pocket allowed to form more favourable complexes. For compounds **13** and **19** their opposite orientation still does not prevent the H-bonds formation between pyridine cycle ring and Arg-120. At the same time compound **3** forms hydrogen bonds between Oxygen of thiazolidine ring with catalytic Ser-530 and between Nitrogen of phenylazo group with Arg-120. Compounds **23** and **34** form complexes with COX-2 on account of Nitrogen of phenylazo group and Oxygen of acetamide moiety with Arg-120 and Tyr-355. The complex between compound **34** and receptor is additionally stabilized by π -H interactions between both thiazolidine and pyridine rings with the lobby residue Leu-93. Compound **35** is deeply bonded within COX-2 active site and therefore Oxygen of acetamide moiety is forming hydrogen-bonding interactions with both Arg-120 and Tyr-355. Finally, compound **36** displays H-bonding interactions between acetamide Oxygen with Arg-120 and Chlorine of dichlorophenyl moiety with Glu-524 at the base of the active site.

Table 7. Interaction mechanisms, amino acid residues of the receptors active centers, interactions types and energy for complexes of thiazolo[4,5-*b*]pyridin-2-ones with COX-1 and COX-2

Compound ID	COX-1				COX-2			
	Ligand atoms and groups participating in the interaction with the receptor, and interaction types	Amino acids residues of the receptor	H-bond distance, Å	Interaction energy, kcal/mol	Ligand atoms and groups participating in the interaction with the receptor, and interaction types	Amino acids residues of the receptor	Bond distance, Å	Interaction energy, kcal/mol
1	=N- <i>Ph</i> , H-acceptor	Arg-120: NE	2.67	0.1	N (pyridine core), H-acceptor	Arg-120: NE	3.41	-0.7
	=N- <i>Ph</i> , H-acceptor	Arg-120: NH2	2.76	-1.6	Thiazolidine core, π -cation	Arg-120: NE	4.70	0.9
	–	–	–	–	Pyridine core, π -H	Tyr-355: OH	4.43	-0.7
2	=N- <i>Ph</i> , H-acceptor	Arg-120: NH1	3.05	-1.2	N (pyridine core),	Arg-120: NE	2.59	0.1
	\equiv N (nitrile group), H-acceptor	Arg120: NH2	2.68	-1.8	Pyridine core, π -H	Tyr-355: OH	4.14	-1.1
6	N (pyridine core), H-acceptor	Arg-120: NH2	3.38	-2.2	N (pyridine core), H-acceptor	Arg-120: NE	3.28	-1.2
	–	–	–	–	Thiazolidine core, π - cation	Arg-120: NE	4.60	-1.3
28	N (pyridine core), H-acceptor	Arg-120: NH2	3.13	-5.2	N (pyridine core), H-acceptor	Tyr-355: OH	2.72	-1.9
	–	–	–	–	=O acetamide group, H-acceptor	Arg-120: NE	2.39	8.5
	–	–	–	–	Pyridine core, π -cation	Arg-120: NH2	4.84	-1.0
35	N (pyridine core),H-acceptor	Arg-120: NH2	3.54	-1.6	=O acetamide group, H-acceptor	Arg-120: NH2	2.49	2.2
	–	–	–	–	=O acetamide group, H-acceptor	Tyr-355: OH	2.59	-0.9
	–	–	–	–	<i>Ph</i> of phenylazo group, π - cation	Lys-83: NZ	3.59	-1.8
36	-N= phenylazo group, H-acceptor	Arg-83 NH1	3.20	-0.7	Cl dichloro-phenylpyrrole fragment, H-donor	Glu-524: OE1	3.00	-2.4
	-N= hydrazide group, H-acceptor	Arg-120 NE	3.05	-3.9	=O acetamide group, H-acceptor	Arg-120: NE	2.67	-5.3
	Pyridine core, Ile-89: CG2 π -H	3.86	-0.8	–	–	–	–	–

3. 2. 2. Docking Results with mPGES-1

mPGES-1 is an inducible and glutathione-dependent enzyme with molecular weight of 15-16 kDa, located on the endoplasmic reticulum. It is a transmembrane homotrimer consisting of 152 amino acid residues long-chain.⁷⁰ Each asymmetric monomer is characterized by a four-helix bundle motif. Thus, the quaternary structure of mPGES-1 consists of a homotrimeric protein complex with twelve membrane-spanning alpha helices, and three

equivalent active site ~15-Å-deep cavities with an opening measuring 12×9 Å within the membrane-spanning region at each monomer interface. The mPGES-1 homotrimer binds three glutathione (GSH) molecules in “U”-shaped geometry due to the strong interactions between its two terminal carboxylic functions and the positively charged residues in the deeper part of the binding site (B:Arg-38, A:Arg-73). The GSH is coordinated by hydrogen bonds involving the side chains of Arg-73, Asn-74,

Glu-77, His-113, Tyr-117, Arg-126, and Ser-127 from helices II and IV, and the side chain of Arg-38 from helix I in a symmetry-related monomer. In addition to the hydrogen bonds, the phenol group of Tyr-130 forms a π -stacking interaction with the gamma peptide linkage between the cysteine and the glutamate side chain of GSH. Several regions in the binding site of mPGES-1 were disclosed which could be targeted by potential ligands. Firstly, it is the binding groove which is located between the GSH binding site and a molecular surface nearby the cytoplasmic part of the protein, mainly composed by aromatic (C:Phe-44, C:His-53) and polar (C:Arg-52) residues. The second binding region is located in a profound cavity corresponding to GSH binding site which is mainly characterized by polar residues. In this area except the side chains residues which coordinate GSH, A:Tyr-130 is important as its phenol group in the side chain is involved in a π -stacking with the gamma peptide linkage between the cysteine and the glutamate of GSH. This key residue could be targeted by a binder through a π - π interaction and/or polar/H-bond interactions with the phenol hydroxyl moiety in the side chain.⁷¹ Also Arg-126 and Ser-127 of chain A represent another fundamental residues in this binding area since they may play a critical role in catalytical isomerization mechanism from PGH2 to PGE2. Finally, moving from the external part of endoplasmic reticulum membrane to the cytoplasmic part of the protein, a binding groove is identifiable at the intersection between chain B and chain A, with polar (A:Gln-134), aliphatic (B:Val-24) and aromatic (B:Tyr-28) residues, and could be bound by long molecular functions.

In recent years a number of synthetic compounds with the property of mPGES-1 inhibition were developed. Significant amount of them belong to fused heterocycles-based derivatives. Among them some mPGES-1 inhibitors also possessing anti-inflammatory action were discovered as phenanthrene imidazoles like MF63,⁷² benzimidazoles,⁷³ indole carboxylic acid derivatives like MK886,⁷⁴ arylpyrrolizines (Licofelone derivatives),⁷⁵ benzoxazoles,⁷⁶ aminobenzothiazoles⁷⁷ and others.

However, despite the high number of inhibitors identified, to date, only two drug candidates are currently in Phase II clinical trials. GS-248 was initiated by Gesynta Pharma AB for treatment of microvascular diseases in chronic inflammatory conditions and is currently being tested in Phase II trial (<https://www.clinicaltrials.gov/search?cond=GS-248>) with systemic sclerosis patients. In 2023 GS-248 has been assigned the non-proprietary substance name vipoglanstat and introduced into clinical phase II development as a drug candidate for treatment of endometriosis. GRC 27864 (Glenmark Pharmaceuticals Ltd.) has successfully passed Phase I of clinical trials and has been adopted for Phase II as dose range finding study to evaluate the safety and efficacy in patients with moderate osteoarthritic pain.⁷⁸ Figure 5 shows chemical structures of some identified mPGES-1 inhibitors.

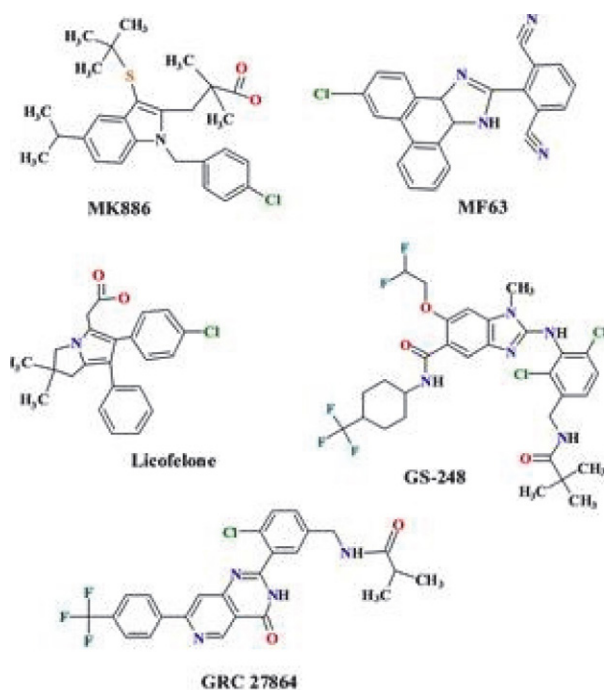


Fig. 5. Chemical structures of some known mPGES-1 inhibitors

In order to identify novel compounds that can inhibit mPGES-1 and to develop a predictive tool for the design of more potent mPGES-1 inhibitors based on thiazolo[4,5-*b*]pyridin-2-one scaffold, we performed docking studies for N³ substituted 5,7-dimethyl-6-phenylazo-3*H*-thiazolo[4,5-*b*]pyridin-2-one derivatives against mPGES-1 considering the X-ray high-resolution (1.2 Å) crystallographic structure of human mPGES-1 linked to GSH (PDB entry code 4AL0). We utilized molecular structures of three known mPGES-1 inhibitors, MK886 (3-(1-(4-chlorobenzyl)-3-methyl-1*H*-indol-2-yl)-2,2-dimethylpropanoic acid), MF63 ([2-(6-Chloro-1*H*-phenanthro[9,10-*dl*imidazol-2-yl)-isophthalonitrile], and Licofelone(2-[2-(4-chlorophenyl)-6,6-dimethyl-1-phenyl-5,7-dihydropyrrolizin-3-yl]acetic acid) as reference ligands. The values of the estimated docking scores for 5,7-dimethyl-6-phenylazo-3*H*-thiazolo[4,5-*b*]pyridin-2-one derivatives and reference drugs in their complexes with mPGES-1 are listed in Table 8.

GBVI/WSA dG, London dG and Alpha HB Scorings for all thiazolo[4,5-*b*]pyridin-2-ones in their complexes with mPGES-1 are comparable with that ones for references, while some compounds exhibit more negative values: compound **21** has more negative values of all three scorings, compounds **25** and **26** are more negative in London dG, compound **35** displays more negative GBVI/WSA dG, and compound **36** has more negative both GBVI/WSA dG and London dG. At the same time Affinity dG Scoring, which estimated the enthalpic contribution to the free energy of binding, has considerably higher negative values

Table 8. The estimated scoring functions for 36 N³ substituted 5,7-dimethyl-6-phenylazo-3*H*-thiazolo[4,5-*b*]pyridin-2-ones and reference drugs in complexes with mPGES-1

Compound ID	GBVI/WSA dG	London dG	Alpha HB	Affinity dG	Compound ID	GBVI/WSA dG	London dG	Alpha HB	Affinity dG
1	-4.813	-4.269	-2.212	-37.696	21	-5.309	-8.062	-5.589	-0.361
2	-3.954	-5.206	-1.289	-54.498	22	-4.042	-6.481	-1.728	-0.281
3	-3.998	-4.104	-1.438	-23.694	23	-4.811	-7.741	-2.422	-24.917
4	-3.376	-4.074	-1.329	-13.094	24	-4.114	-6.827	-1.684	-20.803
5	-3.928	-3.301	-1.452	-23.537	25	-4.017	-10.518	-1.628	-12.337
6	-4.139	-6.594	-1.582	-19.431	26	-4.344	-7.515	-2.389	-24.832
7	-4.068	-6.248	-2.067	-4.959	27	-4.942	-9.528	-1.801	-39.510
8	-3.955	-5.837	-1.566	-19.205	28	-4.879	-5.241	-2.155	-19.550
9	-3.962	-5.844	-1.987	-25.804	29	-5.059	-8.500	-2.345	-15.018
10	-3.656	-6.773	-1.329	-28.648	30	-5.023	-7.287	-3.433	-29.696
11	-4.967	-7.646	-2.943	-7.614	31	-4.950	-6.732	-2.172	-14.517
12	-5.479	-6.173	-3.163	-14.754	32	-4.670	-6.962	-2.199	-42.320
13	-4.432	-6.567	-1.919	-11.702	33	-3.500	-7.511	-0.692	0.000
14	-4.375	-6.311	-1.718	-10.856	34	-4.474	-8.059	-2.675	-13.970
15	-4.209	-8.831	-2.367	-13.734	35	-5.176	-7.469	-3.079	-16.379
16	-4.094	-7.277	-2.611	2.194	36	-5.287	-10.276	-2.616	-15.563
17	-4.607	-6.219	-1.972	-12.391	MK886	-4.040	-7.472	-2.326	-34.163
18	-3.914	-6.593	-1.588	-1.719	MF63	-4.068	-4.599	-1.919	-36.495
19	-4.205	-7.136	-2.109	-31.410	Licofelon	-3.996	-7.811	-2.741	-33.234
20	-4.986	-7.152	-3.149	-14.257					

for the complexes of reference drugs with mPGES-1 in comparison with thiazolo[4,5-*b*]pyridin-2-ones complexed, the exceptions are compounds 1, 2 and 27 with more negative Affinity dG values.

We further analysed the detailed binding modes for mPGES-1 complexes with ligands. The binding orientations and interaction mechanisms in ligand-mPGES-1 complexes for the most active compounds are shown in Table 9.

All ligands fit into the GHS-binding site of mPGES-1, as confirmed by the molecular docking results (Figure 6). Most complexes formation is maintained on account of Arg-126 amino acid residue of mPGES-1 active site interaction with the ligands while ligands' different atoms and functional groups are engaged. For instance, compounds 3, 5, 6, 8, 23 and 27 form hydrogen bonds between Arg-126 and Oxygen of thiazolidine-2-one ring. Additional complexes stabilization may be achieved on ac-

Table 9. Interaction mechanisms, amino acid residues of the receptors active centers, interactions types and energy for complexes of thiazolo[4,5-*b*]pyridin-2-one derivatives with mPGES-1

Compound ID	Ligand atoms and groups participating in the interaction with the receptor, and interaction types	Amino acids residues of the receptor	Bond distance, Å	Interaction energy, kcal/mol
1	N (pyridine core), H-acceptor	Arg-126: NE	3.53	-0.8
	N (pyridine core), H-acceptor	Arg-126: NH2	3.16	-1.2
	=O of thiazolidine-2-one core, H-acceptor	Arg-73: NH2	2.90	-5.7
	=O of thiazolidine-2-one core, H-acceptor	Tyr-117: OH	2.87	-3.2
	-CH ₃ in pyridine core 5 th position, H-π	Tyr-130: 6-ring	4.18	-0.6
2	=O of thiazolidine-2-one core, H-acceptor	Arg-126: NE	2.99	-6.6
	=O of thiazolidine-2-one core, H-acceptor	Arg-126: NH2	3.10	-2.3
	≡N (nitrile group), H-acceptor	Arg-73: NH1	3.38	-2.7
	≡N (nitrile group), H-acceptor	Arg-73: NH2	3.11	-5.7
6	≡N (nitrile group), H-acceptor	Tyr-117: OH	3.33	-2.0
	=O of thiazolidine-2-one core, H-acceptor	Arg-126 NH2	3.02	-4.0
	28	-NH- of hydrazide moiety, H-donor	Thr-131: OG1	3.10
35	Cl dichlorophenyl-furyl fragment, H-donor	Ser-127: OG	3.90	-0.6
	Pyridine core, π-π	Tyr-130: 6-ring	3.93	0.0
36	=N- <i>Ph</i> , H-acceptor	Arg-126: NH2	3.36	-1.3
	Thiazolidine core, π-H	Ser-127: CD	3.87	-1.5

count of H-binding between Nitrogen of nitrile group with Arg-127 and Tyr-117 (compound **2**), hydrogen-bonding interaction between nitro group Oxygen of nitrophenyl moiety in N³ position substituent and Tyr-130 (compound **10**), π -H interaction between pyridine ring and Ser-127 or H- π interaction between Nitrogen in acetamide moiety and Tyr-130 (compounds **4** and **32**, respectively).

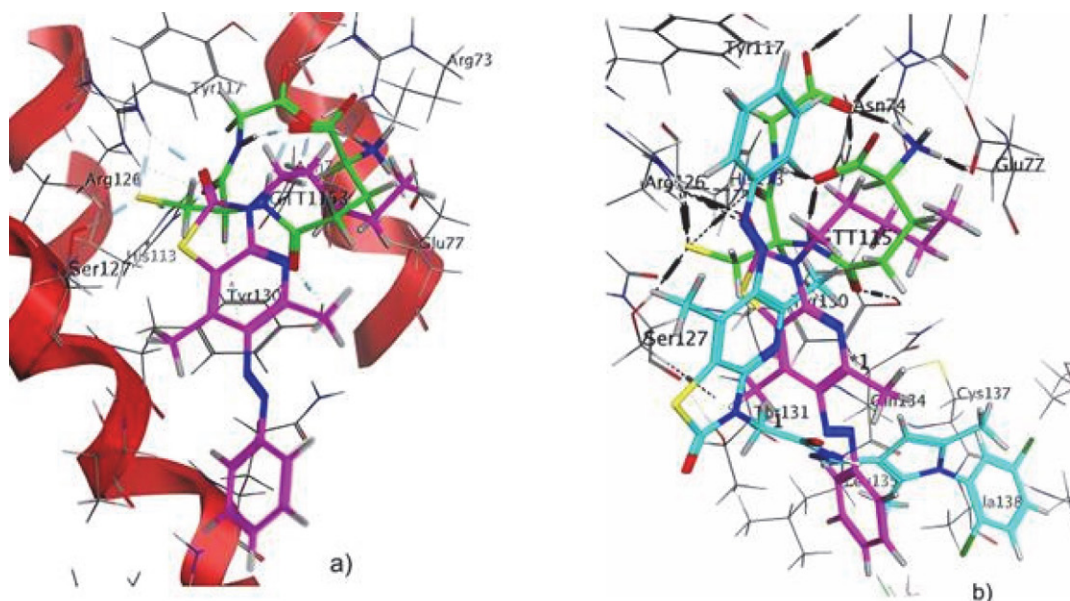


Fig. 6. a) Three-dimensional binding models of compound **6** (magenta) in the GHS-binding site of mPGES-1. The protein is depicted by ribbons (chain A). Glutathione (green) and ligand are represented by sticks; b) Sticks representation of the superposition of GHS (green), compounds **6** (magenta) and **36** (cyan) in mPGES-1 active site

Also, H-bond formation with Arg-126 may be achieved by its interaction with Oxygen of N³-substituent acetamide moiety like in compound **18** complex with mPGES-1. The same Oxygen atom can form hydrogen bonds with Ser-127 (compounds **9**, **31**). For compound **33**, besides Oxygen of acetamide moiety binding with Arg-126, thiazole ring can form π -cation interaction with Arg-126 while compound **19** can form additional hydrogen bond between Oxygen of thiazolidine-2-one ring with Tyr-130. Some compounds are forming hydrogen bonds between Nitrogen of phenyl-azo moiety and Arg-126 amino acid residue as a single binding (compounds **26**, **34**) or in combination with π -H interaction between thiazolidine-2-one ring and Ser-127 (compounds **25**, **36**) accompanied by H- π interaction between Carbon of methyl group in thiazolo[4,5-*b*]pyridin-2-one fused core C⁵ position and Tyr-130 (compounds **13**, **17**, **24**). Arg-126 together with Ser-127 and His-113 may act as H-donors for nitro group Oxygen of nitrophenyl moiety in N³ position substituent (compounds **11**, **12**, **20**, **21**), while additional complexes stabilizing is maintained on account of π -H interactions between thiazolidine-2-one ring (compound **11**), pyridine ring (compound **12**) or phenyl in phenyl-azo fragment (compound **20**) and Tyr-130. Compound **1** can form H-binding with Arg-126 on account of its Nitrogen

of pyridine core. Also hydrogen bonds between Oxygen of acetamide moiety with two amino acids residues – Arg-73 and Tyr-117 exist together with H- π interaction between Carbon of methyl group in thiazolo[4,5-*b*]pyridin-2-one fused core C⁵ position and Tyr-130. For compound **35**, its complex with mPGES-1 is formed on account of hydrogen bonding between Arg-126 and carbonyl Oxygen in benzo-

ic acid moiety accompanied by H-binding between Oxygen of acetamide moiety with Tyr-130 and π -H interaction between thiazolidine-2-one ring with Tyr-130. Some compounds can form π -H interaction between phenyl in phenyl-azo fragment and Arg-126 (compounds **7**, **15**, **22**). In complexes of compounds **15** and **28** with mPGES-1 H-bond is formed between Nitrogen of acetamide moiety and Thr-131, while for compounds **7** and **15** additional π -H interaction between pyridine ring and Ser-127 can stabilize corresponding complexes.

In the complex of compound **22** H-bonding with Thr-131 is forming on account of thiazole core Sulfur atom. Similar S-Thr-131 hydrogen bond is formed for compound **29** in its complex with mPGES-1. Thus compounds **28** and **29** have no interactions with Arg-126. Similarly, compounds **14**, **16** and **35** do not form binding with Arg-126. Compound **14** form H- π interaction between Carbon of methyl group in thiazolo[4,5-*b*]pyridin-2-one fused core C⁵ position with Tyr-130 in combination with π -H interaction between thiazolidine-2-one ring and Ser-127. Compound **16** can form H-bond between Oxygen of acetamide moiety and Tyr-130 in combination with π -H interaction between thiazolidine-2-one ring and Tyr-130. For compound **35** in its complex with mPGES-1 hydrogen bond between Chlorine of dichlorophenyl-furyl fragment

with Ser-127 is accompanied by pyridine ring – Tyr-130 π - π interaction.

Active dock poses of thiazolo[4,5-*b*]pyridines within the binding pocket of mPGES-1 analysis ensured the acceptor-ligand interaction possibility *via* hydrogen binding between oxygen of thiazole ring, Oxygen of N³-substituent acetamide moiety, Nitrogen atom of phenyl-azo moiety or Oxygen of nitrophenyl moiety in N³ position substituent of ligands and key side-chains residues of mPGES-1, confirmed with the effective docking scores.

3. 3. Protein-ligand Interaction Pharmacophore Modelling

A pharmacophore is an abstract description of molecular features that are necessary for molecular recognition of a ligand by a biological macromolecule. The term *pharmacophore* was coined by Paul Ehrlich in 1909 to mean "a molecular framework that carries the essential features responsible for a drug's biological activity".⁷⁹ IUPAC defines a pharmacophore to be "an ensemble of steric and electronic features that is necessary to ensure the optimal supramolecular interactions with a specific biological target and to trigger (or block) its biological response".⁸⁰ So we may consider a pharmacophore as a 3D model describing the type and location of the binding interactions between a ligand and its target receptor. A phar-

macophore model explains how structurally diverse ligands can bind to a common receptor site. Furthermore, pharmacophore models can be used to identify through de novo design or virtual screening novel ligands that will bind to the same receptor.

As a predictive tool for the design of more potent inhibitors discovery we performed 3D pharmacophore modelling for thiazolo[4,5-*b*]pyridines using protein-ligand interaction fingerprints (PLIF) tool implemented in MOE software. PLIFs may be considered as strings that convert protein–ligand interactions from 3D information into 1D representations.

There are two categories of interaction in which a residue may participate in a protein-ligand complex: potential (energy-based) contacts and surface (patch) contacts. For potential contacts, the value is that of the strongest interaction between any pair of atoms in the residue and ligand, whereas for surface contacts the value is the total contact area of each type between a residue and the other molecule.

PLIF possesses a composition of seven visible fingerprint bits: side-chain hydrogen bond donor (*D*), side-chain hydrogen bond acceptor (*A*), backbone hydrogen bond donor (*d*), backbone hydrogen bond acceptor (*a*), solvent hydrogen bond (*O*), ionic attraction (*I*) and surface contact (*C*). The hydrogen bond fingerprints are calculated using a method based on protein contact statistics, where-

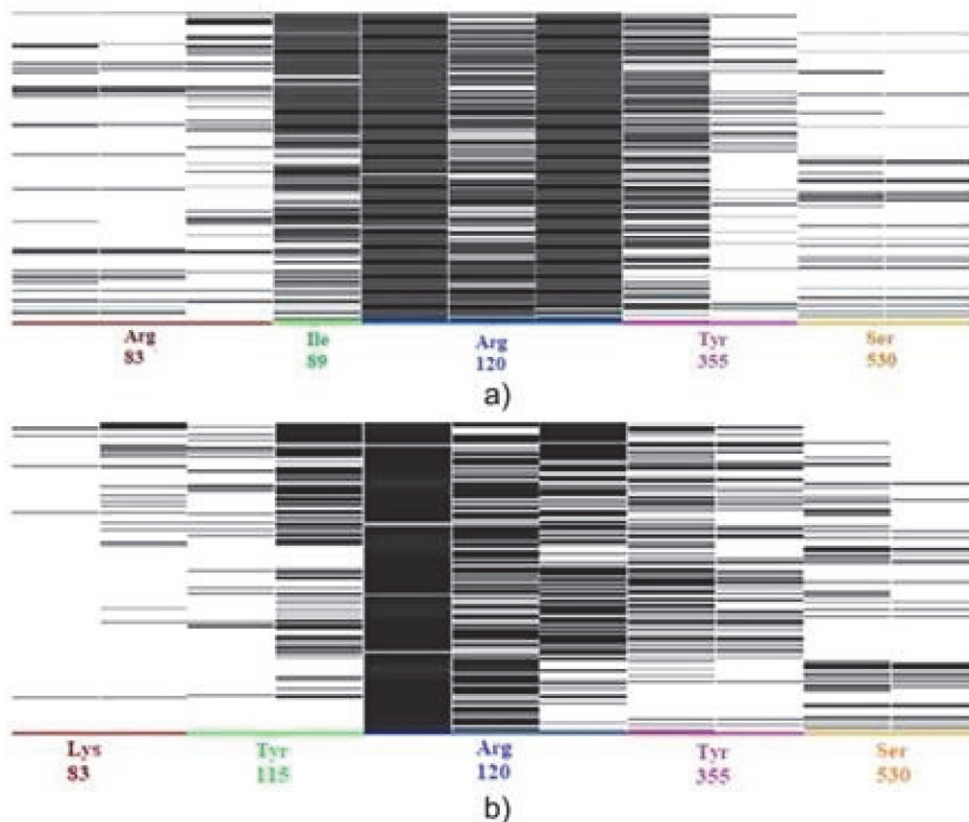


Fig. 7. Barcode representation of the docking interactions between researched compounds and COX-1 (a) and COX-2 (b) isoforms

by a pair of atoms is scored by distance and orientation. Ionic interactions are scored by calculating the inverse square of the distance between atoms with opposite formal charge (e.g. a carboxylate oxygen atom and a protonated amine). Surface contact interactions are determined by calculating the solvent-exposed surface area of the residue, first in the absence of the ligand, then in presence of the ligand.^{81,82}

Receptors interaction fingerprints were generated firstly from the docked poses of the virtual screening hits. Affinity $dG < -4$ was used as a query for active poses. A "barcode" is a matrix image of fingerprints, in which each column corresponds to the formed interaction of a certain type (bit) with the corresponding amino acid residue, amino acid residues are marked on the x-axis. Each line in the "barcode" indicates the active conformational position of the ligand that forms an interaction with the corresponding amino acid residue.

As the interactions summarizing between ligands and both COX isoforms, the barcode diagrams were constructed for the virtual screening hits which depict the most frequent interactions between ligands and the side chains residues of COX-1,2 (Figure 7).

Barcodes for both COX isoforms contain five fingerprints with Arg-83 in COX-1 being changed to Lys-83 in COX-2, also Ile-89 being replaced with Tyr-115. Arg-83 fingerprint in COX-1 barcode consists of 3 bits – AAC, that is it can act as two hydrogen bonds acceptor and may form a surface contact with the ligand. At the same time Lys-83 fingerprint in COX-2 barcode is a two-bits one – AC, acting as hydrogen bond acceptor and forming a surface interaction. Ile-89 fingerprint is one of the most frequently populated in COX-1 barcode while it has just one bit – surface contact. Tyr-115 in COX-2 contains two bits – AC (H-bond acceptor and surface contact). The majority of compounds in the dataset showed interactions with Arg120 residue (99.4% of docking poses for COX-1 and 97.6% of docking poses for COX-2), its fingerprint consists of three bits for both COX isoforms – AAC: it may form two hydrogen bonds with the complexed compound on account of its sidechain nitrogen atoms action as acceptors in the donor-acceptor interactions, and the contact

surface interaction is also possible. The most frequently populated interacting residues are also Tyr355 and Ser-530, both are two-bits fingerprints – AA - acting as two hydrogen bonds acceptors.

The pharmacophore query generator option in the PLIF module was used to generate pharmacophore-3D models from the fingerprint bits with the input setting of 3 Å maximum radius and feature coverage 50% threshold.

Generated pharmacophore models for both COX isoforms included two features (Figure 8).

Each generated model includes one common pharmacophoric feature, which performs a single function in providing binding between ligands and the protein: feature F1 as hydrogen bond acceptor centre (Acc) with the radius of 1.855 Å for COX-1 and hydrophobic centre feature F1 (HydA) with the radius of 2.986 Å for COX-2. The second pharmacophore centre F2 in both obtained queries can perform a dual function: it is a region with the radius of 1.968 Å (COX-1) or 2.259 Å (COX-2) containing an H-acceptor or a hydrophobic atom (Acc&ML|HydA for COX-1 or HydA|Acc&ML for COX-2). Acc&ML means a combination of hydrogen bond acceptor feature and a metal ligation site. The distances between the pharmacophoric centres are 2.81 Å in the model for COX-1 and 6.28 Å in the model for COX-2.

Constructed pharmacophoric models for COX-1,2 were then validated by screening the test compounds database over them. Compounds overlaying with two-points pharmacophore queries (Figure 9) suggests that H-acceptor feature is commonly overlayed with the steric arrangement of the nitrogen atom of the pyridine heterocycle, nitrogen in hydrazide group, or the oxygen atom of the acetamide fragment in N³ substituent moiety. Thiazolidine-2-one core, the carbon atom connected to nitrogen in the 3rd position of the thiazolidine ring, or the carbon atoms of the alkyl substituent in N³ position can act as hydrophobic regions.

Performed pharmacophore search ensured that the pharmacophore queries summary at 357 docking entries obtained for COX-1 are able to describe correctly the absolute hits number of 310 docking conformations (86.83%) with 33 of 36 structures (91.67%) without additional steric



Fig. 8. Two-points pharmacophore queries generated with PLIF tool for thiazolo[4,5-*b*]-pyridin-2-one derivatives in complexes with COX-1 (a) and COX-2 (b)

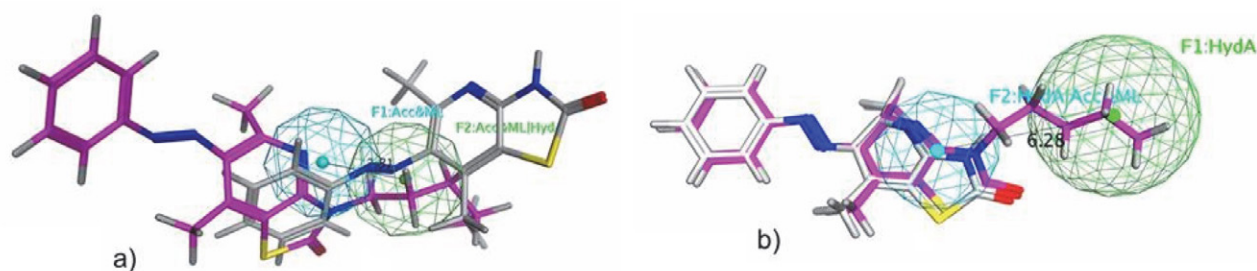


Fig. 9. Two-points pharmacophore queries overlaying with compounds **1** (grey) and **6** (magenta) for COX-1 (a) and COX-2 (b)

modifications of the ligands structure. The correctness of pharmacophore query obtained for COX-2 revealed 23 compounds (63.89%), or 219 conformations (53.16%) out of 412 obtained by docking as the absolute hits. The relative hits number for both COX iso-forms was found 100.00% with the active poses of 36/36 compounds (100.00%).

Receptor interaction fingerprints were generated from the docked poses of the virtual screening hits with mPGES-1 active sites coordinates depicting the interactions between compounds from the dataset and the following receptor amino acids residues: Arg73, His113, Tyr117, Arg126, Ser127, Tyr130, and Thr131 (Figure 10).

Arg-73 fingerprint consists of 2 bits – AC, that is it can act as side-chain hydrogen bond acceptor and may form a surface contact with the ligand. His-113 and Tyr-117 are one-bit fingerprints both acting as hydrogen bond acceptors. The most highly populated Arg-126 amino acid residue and Ser-127 are two-bits fingerprints – AA – both acting as two side-chain hydrogen bonds acceptors. Tyr-130 fingerprint contains 3 bits – AAC, that is it can act as two hydrogen bonds acceptor and may form a surface contact with the ligand. Thr-131 is also a three-bits fingerprint – DDA, while it can act as two side-chain hydrogen bonds donor and may form a surface contact with the ligand.

The generated 3D pharmacophoric model obtained as a result of PLIF identification for thiazolo[4,5-*b*]pyridine-2-one derivatives in mPGES-1 active site contains three common features (Figure 11a): hydrogen bond ac-

ceptor feature with the radius of 2.915 Å and two hydrophobic center features with the radii of 2.768 Å and 2.893 Å. The distances between the H-acceptor and two hydrophobic centres are 6.18 Å and 4.01 Å, and the distance between the hydrophobic pharmacophoric centres is 6.79 Å. The data set compounds were virtual screened over the developed pharmacophore query in order to validate its correctness (Figure 11b). Compounds overlaying with the constructed pharmacophore query for mPGES-1 suggests that H-acceptor feature is commonly overlayed with the nitrogen atom of the pyridine core or the oxygen atom of the acetamide fragment in N³ substituent moiety. Thiazolidine core, the part of pyridine core together with methyl substituents in its 5th or 7th positions, or phenyl moiety connected to azo group can act as hydrophobic regions.

The correctness of pharmacophore queries was confirmed in the way of pharmacophore search performing. The summary at 786 entries showed the absolute hits number of 467 docking conformations (59.41%) with 25 of 36 structures (69.44%). The relative hits number for constructed mPGES-1 pharmacophoric model was found as 786 entries (100.00%) for 36/36 compounds (100.00%).

The analysis of all obtained pharmacophore models indicates the functionality of the condensed bicyclic thiazolopyridine scaffold, which is ensured by the steric placement of atoms of at least one of these heterocycles in the corresponding pharmacophore centers. The generated models can be used to screen virtual compound libraries for potentially active molecules.

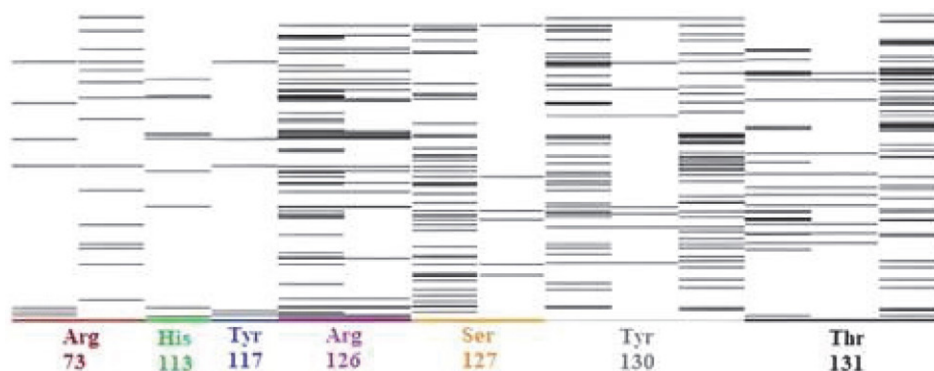


Fig. 10. Barcode representation of the docking interactions between active dock poses of the researched compounds and mPGES-1

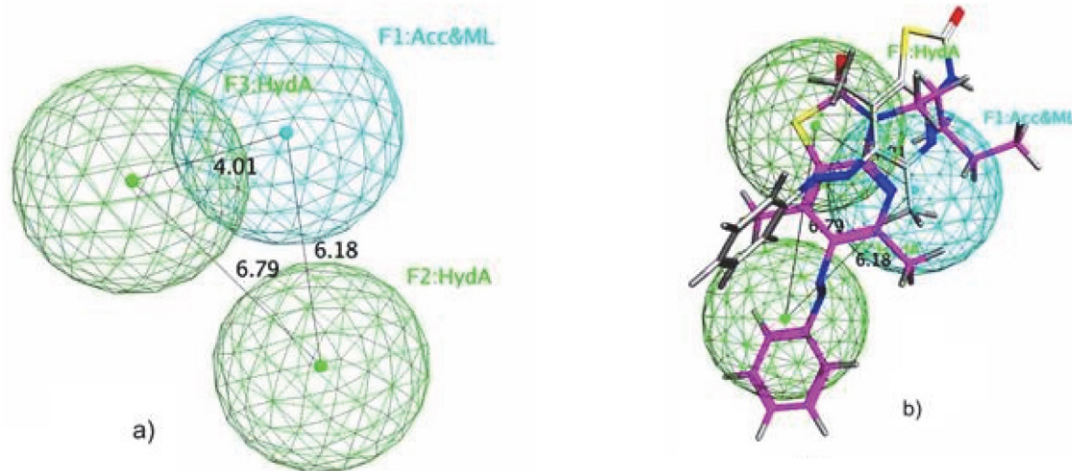


Fig. 11. Three-points pharmacophore query generated with PLIF tool for thiazolo[4,5-*b*]-pyridin-2-ones in complexes with mPGES-1 (a); its overlaying with compounds 1 (grey) and 6 (magenta) (b)

4. Conclusions

Condensed thiazolopyridine heterocyclic system can be considered as a promising scaffold for the combinatorial libraries construction of potential biologically active small molecules. This conclusion is based on the diversity of biological actions possessed by their derivatives and inhibitory properties of this system towards several enzymes, revealed with virtual screening tools, what is typical for privileged structures.

Firstly, the combination of two heterocycles to form a bicyclic condensed system as the scaffold for further functionalization, provides a small number of rotational bonds. Secondly, the affinity of the compounds under study towards several receptors proved by molecular docking results was ensured by the complementarity of the electrostatic and steric surfaces of receptors and ligands in general and the core scaffold in particular, as it was shown that the number of fused bicyclic core heteroatoms were able to form energetically favourable non-covalent interactions with proposed receptors. And, thirdly, the existing possibilities for thiazolopyridine core functionalization, in particular in its 3rd and 6th positions, allow to increase the inhibitory selectivity and specificity of the corresponding derivatives as well as their affinity towards certain receptors by introducing the appropriate substituents into the molecular structure.

The proposed virtual screening results provide an excellent starting point for rational design and *de novo* synthesis of novel thiazolo[4,5-*b*]pyridine-2-one scaffold based potential drug candidates.

Conflict of Interest Statement

The authors confirm that this article content has no conflict of interest.

Acknowledgments

Olena Klenina extends infinite gratitude and appreciation to Authorities of University CEU San Pablo, Madrid, Spain, for opening and funding the position of a researcher within Drug Design and Synthesis research group, School of Pharmacy, she is grateful to the Group Main researcher, Prof. Beatriz de Pascual-Teresa Fernández, and all the Group members, for their solidarity with Ukraine, support, assistance and for the research facilities.

5. References

- H. Tallima, *ACS Omega* **2021**, *6*, 15559–15563. DOI:10.1021/acsomega.1c01952
- B. Wang, L. Wu, J. Chen, L. Dong, C. Chen, Z. Wen, J. Hu, I. Fleming, D.W. Wang, *Signal Transduct Target Ther.* **2021**, *6*, 94. DOI:10.1038/s41392-020-00443-w
- A. K. Chakraborti, S.K. Garg, R. Kumar, H.F. Motiwala, P.S. Jadhavar, *Curr. Med. Chem.* **2010**, *17*, 1563–1593. DOI:10.2174/092986710790979980
- C. Sostres, C.J. Gargallo, M.T. Arroyo, A. Lanás, *Best Pract. Res. Clin. Gastroenterol.* **2010**, *24*, 121–132. DOI:10.1016/j.bpg.2009.11.005
- J. K. Norberg, E. Sells, H.H. Chang, S.R. Alla, S. Zhang, E.J. Meuillet, *Pharm. Pat. Anal.* **2013**, *2*, 265–288. DOI:10.4155/ppa.12.90
- Q. Wang, Y. Li, M. Wu, S. Huang, A. Zhang, Y. Zhang, Z. Jia, *Am. J. Transl. Res.* **2021**, *13*, 391–419.
- T. Chaban, O. Klenina, I. Chaban, V. Ogurtsov, S. Harkov, M. Lelyukh, *Pharmacia* **2018**, *65*, 54–70.
- A. Moran, E. Martin, C. Velasco, M.L. Martin, L. San Roman, E. Caballero, P. Puebla, M. Medarde, A. San Feliciano, *J. Pharm. Pharmacol.* **1997**, *49*, 421–425. DOI:10.1111/j.2042-7158.1997.tb06817.x

9. O. Klenina, T. Chaban, T. B. Zimenkovsky, S. Harkov, V. Ogurtsov, T. Chaban, I. Myrko, *Pharmacia* **2017**, *64*, 49–71.
10. I. M. Othman, M. A. Gad-Elkareem, H. A. Radwan, R. Badraoui, K. Aouadi, M. Snoussi, A. Kadri, *ChemistrySelect* **2021**, *6*, 7860–7872. DOI:10.1002/slct.202101622
11. H. K. A. El-Mawgoud, *Chem. Pharm. Bull.* **2019**, *67*, 1314–1323. DOI:10.1248/cpb.c19-00681
12. R. Nurugan, S. Anbazhagan, S. Sriman Narayanan, *Eur. J. Med. Chem.* **2009**, *44*, 3272–3279. DOI:10.1016/j.ejmech.2009.03.035
13. V. Kamat, R. Santosh, B. Poojary, S.P. Nayak, B.K. Kumar, M. Sankaranarayanan, Faheem, S. Khanapure, D.A. Barretto, S.K. Vootla, *ACS Omega* **2020**, *5*, 25228–25239. DOI:10.1021/acsomega.0c03386
14. T. Chaban, O. Klenina, I. Drapak, V. Ogurtsov, I. Chaban, V. Novikov, *Chem. Chem. Technol.* **2014**, *89*, 287–292. DOI:10.23939/chcht08.03.287
15. S. G. Hegde, M.D. Mahoney, *J. Agric. Food Chem.* **1993**, *41*, 2131–2134. DOI:10.1021/jf00035a058
16. T. I. Chaban, R. R. Panchuk, O. V. Klenina, N. R. Skorokhyd, V. V. Ogurtsov, I. G. Chaban, *Biopolym. Cell* **2012**, *28*, 389–396. DOI:10.7124/bc.000075
17. A. U. Rao, A. Palani, X. Chen, Y. Huang, R. G. Aslanian, R. E. West Jr, S. M. Williams, R.-L. Wu, J. Hwa, C. Sondey, J. Lachowicz, *Bioorganic Med. Chem. Lett.* **2009**, *19*, 6176–6180. DOI:10.1016/j.bmcl.2009.09.006
18. L. Xia, Y. Zhang, J. Zhang, S. Lin, K. Zhang, H. Tian, Y. Dong, H. Xu, *Molecules* **2020**, *25*, 4630. DOI:10.3390/molecules25204630
19. G. R. Bebernitz, V. Beaulieu, B. A. Dale, R. Deacon, A. Duttaroy, J. Gao, M. S. Grondine, R. C. Gupta, M. Kakmak, M. Kavana, L. C. Kirman, J. Liang, W. M. Maniara, S. Munshi, S. S. Nadkarni, H. F. Schuster, T. Stams, I. St Denny, P. M. Taslimi, B. Vash, S. L. Caplan, *J. Med. Chem.* **2009**, *52*, 6142–6152. DOI:10.1021/jm900839k
20. R. Mohareb, F. Al-Omran, M. Abdelaziz, R. Ibrahim, *Acta Chim. Slov.* **2017**, *64*, 349–364. DOI:10.17344/acsi.2017.3200
21. M. Ahmadi, S. Bekeschus, K.D. Weltmann, T. von Woedtke, K. Wende, *RSC Med. Chem.* **2022**, *13*, 471–496. DOI:10.1039/D1MD00280E
22. M. M. El-Kerdawy, M. A. Ghaly, S. A. Darwish, H. A. Abdel-Aziz, A. R. Elsheakh, R. S. Abdelrahman, G. S. Hassan, *Bioorg. Chem.* **2019**, *83*, 250–261. DOI:10.1016/j.bioorg.2018.10.048
23. L. Y. He, S. S. Zhang, D. X. Peng, L. P. Guan, S. H. Wang, *Bioorganic Med. Chem. Lett.* **2020**, *30*, 127376. DOI:10.1016/j.bmcl.2020.127376
24. B. Smith, H. H. Chang, F. Medda, V. Gokhale, J. Dietrich, A. Davis, E. J. Meuillet, C. Hulme, *Bioorganic Med. Chem. Lett.* **2012**, *22*, 3567–3570. DOI:10.1016/j.bmcl.2012.03.013
25. T. Hanke, F. Dehm, S. Liening, S. D. Popella, J. Maczewsky, M. Pillong, J. Kunze, C. Weinigel, D. Barz, A. Kaiser, M. Wurglics, M. Lämmerhofe, G. Schneider, L. Sautebin, M. Schubert-Zsilavec, O. Werz, *J. Med. Chem.* **2013**, *56*, 9031–9044. DOI:10.1021/jm401557w
26. HyperChem package Release 7.5 for Windows, Hypercube, Inc., 1115 NW 4th Street, Gainesville, Florida 32601, USA. <http://www.hyper.com>
27. I. V. Tetko, J. Gasteiger, R. Todeschini, A. Mauri, D. Livingstone, P. Ertl, V. A. Palyulin, E. V. Radchenko, N. S. Zefirov, A. S. Makarenko, V. Y. Tanchuk, V. V. Prokopenko, *J. Comput. Aided Mol. Des.* **2005**, *19*, 453–463. DOI:10.1007/s10822-005-8694-y
28. A. Golbraikh, M. Shen, Z. Xiao, Y. D. Xiao, K. H. Lee, A. Tropsha, *J. Comput. Aided Mol. Des.* **2003**, *17*, 241–253. DOI:10.1023/A:1025386326946
29. D. B. de Oliviera, A. C. Gaudio. *Quant. Struct. Act. Relat.* **2000**, *19*, 599–601. DOI:10.1002/1521-3838(200012)19:6<599::AID-QSAR599>3.0.CO;2-B
30. M. M. Suleiman, S. G. Isaev, O. V. Klenina, V. V. Ogurtsov, *J. Chem. Pharm. Res.* **2014**, *6*, 1219–1235. DOI:10.1023/A:1025386326946
31. O. Ouattara, T. S. Affi, M. G. - R. Koné, K. Bamba, N. Ziao, *Int. J. Eng. Res. Appl.* **2017**, *7*, 50–56. DOI:10.9790/9622-0705015056
32. A. Golbraikh, A. Tropsha, *J. Mol. Graph. Model.* **2002**, *20*, 269–276. DOI:10.1016/S1093-3263(01)00123-1
33. N. Chirico, P. Gramatica, *J. Chem. Inf. Model.* **2011**, *51*, 2320–2335. DOI:10.1021/ci200211n
34. R. Kiralj, M. Ferreira, *J. Braz. Chem. Soc.* **2009**, *20*, 770–787. DOI:10.1590/S0103-50532009000400021
35. Molecular Operating Environment (MOE), 2012.10; Chemical Computing Group Inc., 1010 Sherbooke St. West, Suite #910, Montreal, QC, Canada, H3A 2R7, 2012.
36. S. Vilar, G. Cozza, S. Moro, *Curr. Top. Med. Chem.* **2008**, *8*, 1555–1572. DOI:10.2174/156802608786786624
37. N. M. O’Boyle, M. Banck, C. A. James, C. Morley, T. Vandermeersch, G.R. Hutchison, *J. Cheminform.* **2011**, *3*, 1–14. DOI:10.1186/1758-2946-3-33
38. K. Gupta, B. S. Selinsky, C. J. Kaub, A. K. Katz, P. J. Loll, *J. Mol. Biol.* **2004**, *335*, 503–518. DOI:10.1016/j.jmb.2003.10.073
39. K. C. Duggan, M. J. Walters, J. Musee, J. M. Harp, J. R. Kiefer, J. A. Oates, L. J. Marnett, *J. Biol. Chem.* **2010**, *285*, 34950–34959. DOI:10.1074/jbc.M110.162982
40. T. Sjögrena, J. Nordb, M. Eka, P. Johanssona, G. Liub, S. Geschwindnera, *PNAS* **2013**, *110*, 3806–3811. DOI:10.1073/pnas.1218504110
41. T. Chaban, O. Klenina, S. Harkov, V. Ogurtsov, I. Chaban, I. Nekttegaev, *Pharmacia* **2017**, *64*, 16–30.
42. T. I. Chaban, O. V. Klenina, B. S. Zimenkovsky, I. G. Chaban, V. V. Ogurtsov, L. S. Shelepeten, *Der Pharma Chem.* **2016**, *8*, 534–542.
43. R. Kiralj, M. Ferreira, *J. Braz. Chem. Soc.* **2009**, *20*, 770–787. DOI:10.1590/S0103-50532009000400021
44. V. Consonni, D. Ballabio, R. Todeschini, *J. Chemom.* **2010**, *24*, 194–201. DOI:10.1002/cem.1290
45. P. Gramatica, *IJQSPR* **2020**, *5*, 61–97. DOI:10.4018/IJQSPR.20200701.0a1
46. A. M. Helguera, R. D. Combes, M. P. Gonzalez, M. N. D. S. Cordeiro, *Curr. Top. Med. Chem.* **2008**, *8*, 1628–1655. DOI:10.2174/156802608786786598
47. A. Mauri, V. Consonni, R. Todeschini, R. Molecular Descriptors. In: J. Leszczynski, A. Kaczmarek-Kedziera, T. Puzyn, M.

- G. Papadopoulos, H. Reis, M. K. Shukla (Eds.): Handbook of Computational Chemistry, Springer, Cham., Switzerland, 2017, pp. 2079–2082. DOI:10.1007/978-3-319-27282-5_51
48. T. Grosser, S. Fries, G. A. FitzGerald, *J. Clin. Investig.* **2006**, *116*, 4–15. DOI:10.1172/JCI27291
49. T. Brzozowski, P. C. Konturek, S. J. Konturek, Z. Sliwowski, R. Pajdo, D. Drozdowicz, A. Ptak, E. G. Hahn, *Microsc. Res. Tech.* **2001**, *53*, 343–353. DOI:10.1002/jemt.1102
50. K. N. Khan, S. K. Paulson, K. M. Verburg, J. B. Lefkowitz, T. J. Maziasz, *Kidney Int.* **2002**, *61*, 1210–1219. DOI:10.1046/j.1523-1755.2002.00263.x
51. R. D. Puspita, D. M. Rizal, R. A. Syarif, I. P. Sari, *Open Access Maced. J. Med. Sci.* **2023**, *11(F)*, 31–37. DOI:10.3889/oamjms.2023.9123
52. T. J. Maier, K. Schilling, R. Schmidt, G. Geisslinger, S. Grösch, *Biochem. Pharmacol.* **2004**, *67*, 1469–1478. DOI:10.1016/j.bcp.2003.12.014
53. T. Kamijo, T. Sato, Y. Nagatomi, T. Kitamura, *Int. J. Urol.* **2001**, *8*, S35–S39. DOI:10.1046/j.1442-2042.2001.00332.x
54. M. J. Czachorowski, A. F. S. Amaral, S. Montes-Moreno, J. Lloreta, A. Carrato, A. Tardón, M. M. Morente, M. Kogevinas, F. X. Real, N. Malats, *PLOS ONE* **2012**, *7*, e45025. DOI:10.1371/journal.pone.0045025
55. L. G. Howes, *Ther Clin Risk Manag.* **2007**, *3*, 831–845.
56. F. Bergqvist, R. Morgenstern, P.-J. Jakobsson, *Prostaglandins Other Lipid Mediat.* **2020**, *147*, 106383. DOI:10.1016/j.prostaglandins.2019.106383
57. M. Thulasingham, L. Orellana, E. Nji, S. Ahmad, A. Rinaldo-Matthis, J. Z. Haeggström, *Nat. Commun.* **2021**, *12*, 1728–1739. DOI:10.1038/s41467-021-21924-8
58. K. Scholich, G. Geisslinger, *Trends Pharmacol. Sci.* **2006**, *27*, 399–401. DOI:10.1016/j.tips.2006.06.001
59. J. Z. Haeggström, C. D. Funk, *Chem. Rev.* **2011**, *111*, 5866–5898. DOI:10.1021/cr200246d
60. J. Steinmetz-Späh, P. J. Jakobsson, *Expert Opin. Ther. Targets* **2023**, *27*, 1115–1123. DOI:10.1080/14728222.2023.2285785
61. A. L. Blobaum, L. J. Marnett, *J. Med. Chem.* **2007**, *50*, 1425–1441. DOI:10.1021/jm0613166
62. U. R. Mbonye, C. Yuan, C. E. Harris, R. S. Sidhu, I. Song, T. Arakawa, W. L. Smith, *Biol. Chem.* **2008**, *283*, 8611–8623. DOI:10.1074/jbc.M710137200
63. J. J. Prusakiewicz, K. C. Duggan, C. A. Rouzer, L. J. Marnett, *Biochemistry* **2009**, *48*, 7353–7355. DOI:10.1021/bi900999z
64. A. S. Felts, C. Ji, J. B. Stafford, B. C. Crews, P. J. Kingsley, C. A. Rouzer, M. K. Washington, K. Subbaramaiah, B. S. Siegel, S. M. Young, A. J. Dannenberg, L. J. Marnett, *ACS Chem. Biol.* **2007**, *2*, 479–483. DOI:10.1021/cb700077z
65. F. J. Van Der Ouderaa, M. Buytenhek, D. H. Nugteren, D. A. Van Dorp, *Eur. J. Biochem.* **1980**, *109*, 1–8. DOI:10.1111/j.1432-1033.1980.tb04760.x
66. P. J. Loll, C. T. Sharkey, S. J. O'Connor, C. M. Dooley, E. O'Brien, M. Devocelle, K. B. Nolan, B. S. Selinsky, D. J. Fitzgerald, *Mol. Pharmacol.* **2001**, *60*, 1407–1413. DOI:10.1124/mol.60.6.1407
67. S. W. Rowlinson, J. R. Kiefer, J. J. Prusakiewicz, J. L. Pawlitz, K. R. Kozak, A. S. Kalgutkar, W. C. Stallings, R. G. Kurumbail, L. J. Marnett, *J. Biol. Chem.* **2003**, *278*, 45763–45769. DOI:10.1074/jbc.M305481200
68. J. A. Mancini, D. Riendeau, J. P. Falguyret, P. J. Vickers, G. P. O'Neill, *J. Biol. Chem.* **1995**, *270*, 29372–29377. DOI:10.1074/jbc.270.49.29372
69. J. J. Prusakiewicz, A. S. Felts, B. S. Mackenzie, L. J. Marnett, *Biochemistry* **2004**, *43*, 15439–15445. DOI:10.1021/bi048534q
70. T. Sjögren, J. Nord, M. Ek, P. Johansson, G. Liu, S. Geschwindner, *PNAS* **2013**, *110*, 3806–3811. DOI:10.1073/pnas.1218504110
71. G. Lauro, M. Manfra, S. Pedatella, K. Fischer, V. Cantone, S. Terracciano, A. Bertamino, C. Ostacolo, I. Gomez-Monterrey, M. De Nisco, R. Riccio, E. Novellino, O. Werz, P. Campiglia, G. Bifulco, *Eur. J. Med. Chem.* **2017**, *125*, 278–287. DOI:10.1016/j.ejmech.2016.09.042
72. D. Xu, S. E. Rowland, P. Clark, A. Giroux, B. Côté, S. Guiral, M. Salem, Y. Ducharme, R. W. Friesen, N. Méthot, J. Mancini, L. Audoly, D. Riendeau, *J. Pharmacol. Exp. Ther.* **2008**, *326*, 754–763. DOI:10.1124/jpet.108.138776
73. N. Muthukaman, M. Tambe, S. Deshmukh, D. Pisal, S. Tondlekar, M. Shaikh, N. Sarode, V. G. Kattige, M. Pisat, P. Sawant, S. Honnegowda, V. Karande, A. Kulkarni, D. Behera, S. B. Jadhav, R. R. Sangana, G. S. Gudi, N. Khairatkar-Joshi, L. A. Gharat, *Bioorg. Med. Chem. Lett.* **2017**, *27*, 5131–5138. DOI:10.1016/j.bmcl.2017.10.062
74. D. Riendeau, R. Aspiotis, D. Ethier, Y. Gareau, E. L. Grimm, J. Guay, S. Guiral, H. Juteau, J. A. Mancini, N. Méthot, J. Rubin, R. W. Friesen, *Bioorg Med Chem Lett.* **2005**, *15*, 3352–3355. DOI:10.1016/j.bmcl.2005.05.027
75. A. Koeberle, U. Siemoneit, U. Bühring, H. Northoff, S. Laufer, W. Albrecht, O. Werz, *J. Pharmacol. Exp. Ther.* **2008**, *326*, 975–982. DOI:10.1124/jpet.108.139444
76. N. Kablaoui, S. Patel, J. Shao, D. Demian, K. Hoffmaster, F. Berlioz, M. L. Vazquez, W. M. Moore, R. A. Nugent, *Bioorg. Med. Chem. Lett.* **2013**, *23*, 907–911. DOI:10.1016/j.bmcl.2012.10.040
77. M. G. Chini, A. Giordano, M. Potenza, S. Terracciano, K. Fischer, M. C. Vaccaro, E. Colarusso, I. Bruno, R. Riccio, A. Koeberle, O. Werz, G. Bifulco, *ACS Med. Chem. Lett.* **2020**, *1*, 783–789. DOI:10.1021/acsmchemlett.9b00618
78. S. Sant, M. Tandon, V. Menon, N. Khairatkar Joshi, K. Korukonda, O. Levine-Dolberg, *Osteoarthr. Cartil.* **2018**, *26*, S351–S352. DOI:10.1016/j.joca.2018.02.698
79. P. Ehrlich, *Ber. Dtsch. Chem. Ges.* **1909**, *42*, 17–47. DOI:10.1002/cber.19090420105
80. C. G. Wermuth, C. R. Ganellin, P. Lindberg, L. A. Mitscher, *Pure Appl. Chem.* **1998**, *70*, 1129–1143. DOI:10.1351/pac199870051129
81. N. H. N. Moorthy, S. F. Sousa, M. J. Ramos, P. A. Fernandes, *J. Enzyme Inhib. Med. Chem.* **2016**, *31*, 1428–1442. DOI:10.3109/14756366.2016.1144593
82. N. H. N. Moorthy, N. M. Cerqueira, M. J. Ramos, P. A. Fernandes, *Chemom. Intell. Lab. Syst.* **2015**, *140*, 102–116. DOI:10.1016/j.chemolab.2014.11.009

Povzetek

Poročamo o kombinirani in silico strategiji za raziskovanje molekularnih mehanizmov serije 3H-tiazolo[4,5-b]piridin-2-onov, ki kažejo močno protieksudativno delovanje. Pri raziskavi smo uporabili metode QSAR, molekularnega sidranja in modeliranja farmakoforov. Pri generiranju QSAR modelov z deskriptorji 2D avtokorelacije smo uporabili tehniko GA-ML. Eno- in dvo-parametrski regresiji je razkrila, da določeni strukturni vzorci ali heteroatomi vzajemno prispevajo k povečanju protieksudativne aktivnosti. Možne mehanizme delovanja smo določili s fleksibilnimi simulacijami sidranja v encime, ki nastopajo v poti ciklooksigenaze (COX-1, COX-2, mPGES-1). Rezultati kažejo na možnost tvorbe stabilnih kompleksov z dobrimi ocenami sidranja in pravilno orientacijo ligandov znotraj aktivnih mest encimov. Modeliranje farmakoforov je bilo izvedeno z uporabo metodologije prstnih odtisov interakcij med proteinom in ligandom. Napravili smo 3D farmakoforne preiskave z dvema in tremi centri. Njihova analiza je nakazala funkcionalnost bicikličnega tiazolopiridinskega ogrodja, kar dokazuje, da so heteroatomi sterično umeščeni v ustrezne farmakoforne centre.



Except when otherwise noted, articles in this journal are published under the terms and conditions of the Creative Commons Attribution 4.0 International License